AD-A122 262 COMPOSITE MATERIALS FOR STRUCTURAL DESIGN(U) TEXAS A AND M UNIV COLLEGE STATION MECHANICS AND MATERIALS RE.. W L BRADLEY ET AL. MAR 82 MM-3724-82-1 AFOSR-TR-82-1018 1/2

UNCLASSIFIED F49620-78-C-0034 F/G 11/4 NL

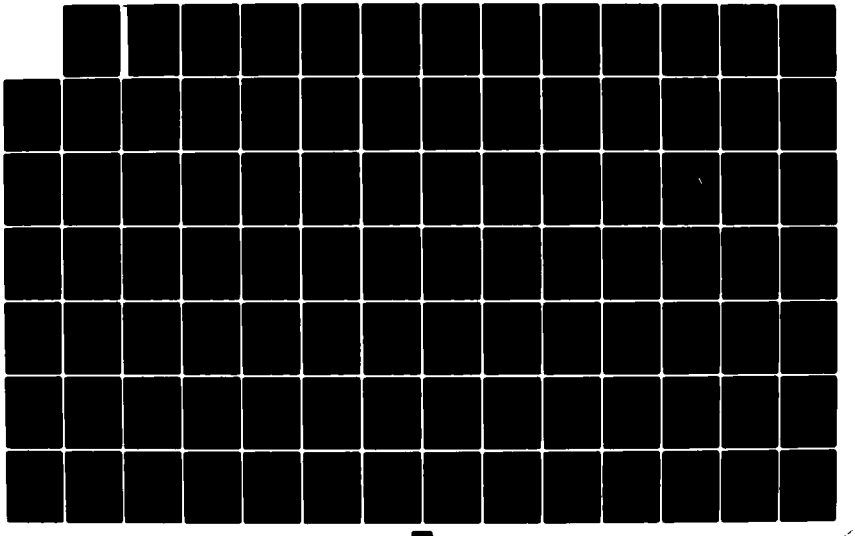

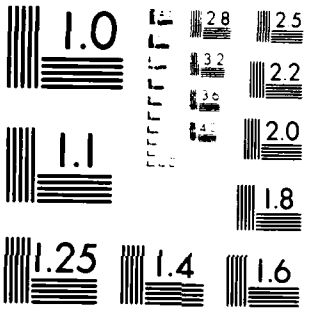

Mechanics and Materials Center
TEXAS A&M UNIVERSITY
College Station, Texas

Final

COMPOSITE MATERIALS FOR STRUCTURAL DESIGN

(FOURTH ANNUAL TECHNICAL REPORT)

AIR FORCE OFFICE OF SCIENTIFIC RESEARCH
OFFICE OF AEROSPACE RESEARCH
UNITED STATES AIR FORCE
CONTRACT NO. F49620-78-C-0034

MM 3724-82-1
MARCH 1982

COMPOSITE MATERIALS FOR STRUCTURAL DESIGN

Fourth Annual Technical Report

by the

Professional Staff

of the

TEXAS A&M UNIVERSITY

MECHANICS AND MATERIALS CENTER

Submitted to the

Air Force Office of Scientific Research

Office of Aerospace Research

United States Air Force

MM 3724-82-1

Contract No. F49620-78-C-0034

March 1982

UNCLASSIFIED

SECURITY CLASSIFICATION OF THIS PAGE *(When Data Entered)*

REPORT DOCUMENTATION PAGE		READ INSTRUCTIONS BEFORE COMPLETING FORM
1. REPORT NUMBER AFOSR-TR- 82-1018	2. GOVT ACCESSION NO. A122 262	3. RECIPIENT'S CATALOG NUMBER
4. TITLE *(and Subtitle)* COMPOSITE MATERIALS FOR STRUCTURAL DESIGN		5. TYPE OF REPORT & PERIOD COVERED FINAL 1 Jan 81 - 31 Dec 81
		6. PERFORMING ORG. REPORT NUMBER
7. AUTHOR(s) W L BRADLEY, W E HAISLER, J S HAM, R A SCHAPERY, Y WEITSMAN		8. CONTRACT OR GRANT NUMBER(s) F49620-78-C-0034
9. PERFORMING ORGANIZATION NAME AND ADDRESS TEXAS A&M UNIVERSITY MECHANCIS & MATERIAIS CENTER COLLEGE STATION, TX 77843		10. PROGRAM ELEMENT, PROJECT, TASK AREA & WORK UNIT NUMBERS 61102F 2307/B2
11. CONTROLLING OFFICE NAME AND ADDRESS AIR FORCE OFFICE OF SCIENTIFIC RESEARCH/NA BOLLING AFB, DC 20332		12. REPORT DATE March 1982
		13. NUMBER OF PAGES 84
14. MONITORING AGENCY NAME & ADDRESS*(if different from Controlling Office)*		15. SECURITY CLASS. *(of this report)* UNCLASSIFIED
		15a. DECLASSIFICATION DOWNGRADING SCHEDULE

16. DISTRIBUTION STATEMENT *(of this Report)*

Approved for Public Release; Distribution Unlimited.

17. DISTRIBUTION STATEMENT *(of the abstract entered in Block 20, if different from Report)*

18. SUPPLEMENTARY NOTES

19. KEY WORDS *(Continue on reverse side if necessary and identify by block number)*

COMPOSITE MATERIALS	DELAMINATION	FRACTURE
RESINS	RESIDUAL STRESSES	DAMAGE
ADHESIVES	VISCOELASTICITY	

20. ABSTRACT *(Continue on reverse side if necessary and identify by block number)*

Research activities related to advanced fiber reinforced plastics are reported in detail for the final year of the initial contract on the continuing composites program at Texas A&M. ~~Detailed~~ reports for earlier ~~years~~ are available and referenced. ~~During~~ this final contract year work was initiated or continued in the areas of fracture, delamination, fatigue, and residual stresses in elastic and viscoelastic composites. Delamination fracture toughness is investigated using macroscopic measurements of fracture toughness to determine critical energy release rate for crack propagation

DD FORM 1 JAN 73 1473 EDITION OF 1 NOV 65 IS OBSOLETE

UNCLASSIFIED

SECURITY CLASSIFICATION OF THIS PAGE *(When Data Entered)*

and is interpreted in terms of microscopic mechanisms of fracture determined from careful examination of the fracture surface using a scanning electron microscope. Additional experimental work in compression-induced delamination and delamination under complex load histories is presented. Analytical methods are developed for prediction of the mechanical state and energy release rate for delamination and used in the investigation of tensile coupons with various amounts of delamination and matrix degradation due to microcracking. A viscoelastic crack growth theory for nonlinear media was developed earlier in the program and this work is being extended to develop a damage theory of laminates. An investigation of the effects of moisture and temperature on residual stresses in composite laminates is continuing. Solution forms which relate curvatures in unsymmetric cross-ply laminates to temperature excursions and moisture content, including viscoelastic effects, were formulated and programmed. Using this work a theoretical investigation was conducted on optimal cool-down paths for minimizing residual stress in cross-ply laminates and adhesive joints. An investigation of shear deformation effects shows that sharp spatial variations of external loads may cause very significant shear effects, sufficient to invalidate the results of classical plate theory even for thin laminates. Also classical plate theory may grossly under-predict the amount of material damping available due to the viscoelasticity of the resin. A mechanics formulation was initiated to represent damage growth in polymeric resins due to crazing prior to cracking. A nonlinear viscoelastic finite element program based on the theory of Schapery has been developed. Limited comparison with experimental data indicates relatively good correlation for nonmetals and some metals at elevated temperature. An attempt was made to determine the effects of aging for a series of thermoset epoxy resins using differential scanning calorimetry. The effects identified to date are small and buried in experimental noise. A study has been initiated seeking resin molecular parameters likely to be related to toughness but no relationship has yet been identified. A molecular model for resin creep is in the early stages of development. Activities of all faculty members are listed, and abstracts of seven M.S. theses and two papers describing recently completed work are included.

TABLE OF CONTENTS

TABLE OF CONTENTS (cont.)

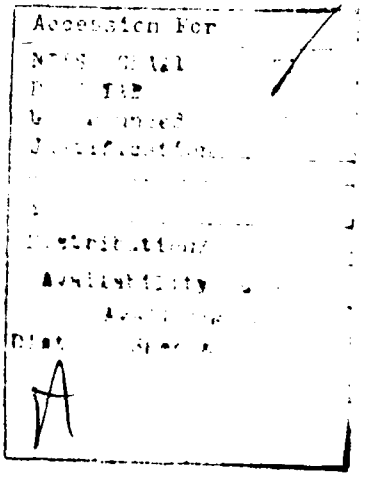

1. INTRODUCTION

1.1 Summary

Primary activities during 1981 consisted of (i) expanding the laboratory capabilities for processing and testing of polymeric composites, especially by integrating automated data acquisition equipment with laboratory instruments and developing software for acquiring and analyzing data; (ii) conducting research in accordance with the Statement of Work given in Section 1.2; (iii) preparing nine technical papers and M.S. theses; and (iv) various interactions of the faculty with the technical community through presentation of papers, participation as members of technical committees, etc. Reference [1] summarizes work done in 1980.

Sections 2-7 summarize the research activities. The professional personnel associated with the project and outside activities of the faculty related to composites are given in Section 8. Additional material on completed work and student activities is in the Appendices.

1.2 Statement of Work

"a. Investigate the effects of cure cycle parameters on mechanical characteristics of resins, composites and composite structural specimens:

(1) Study the curing process.

(2) Investigate the effects of cure cycle parameters on physical aging.

(3) Investigate generation, relief and effects of residual stresses in laminates.

b. Investigate deformation, damage growth and fracture behavior for resins, composites and composite structural specimens:

(1) Develop and verify constitutive equations.

(2) Develop and verify ply damage and delamination models.

(3) Develop an automated structural material property characterization system and data base."

2. MATRIX CONTROLLED FRACTURE BEHAVIOR OF GRAPHITE/EPOXY COMPOSITES*

2.1 Introduction

It is now recognized that delamination cracking is a serious problem for some applications of graphite/epoxy composites. It is therefore important to characterize the delamination fracture toughness. Typically, both tensile and shear stresses exist on the fracture plane, and thus various combinations of tension and shear have to be studied in mixed-mode fracture tests. Furthermore, a better understanding of how the fracture of the epoxy is effected by the presence of the graphite fibers is needed so intrinsic toughness in the material system may be fully realized by proper adjustments in processing that effect the thickness of the resin rich region, fiber waviness, etc.

The purpose of this research has been to better understand the fracture behavior of graphite/epoxy composites when the crack path is principally through the epoxy matrix. Macroscopic measurements of fracture toughness have been made to determine the critical energy release rate for crack propagation. These have been interpreted in terms of microscopic mechanisms of fracture determined from a careful examination of the fracture surface using a scanning electron microscope.

The majority of the research in this area is detailed in the two M.S. Theses (cf. Section 7 for Abstracts):

(i) "Mode I-Mode II Delamination Fracture Toughness of a Unidirectional Graphite/Epoxy Composite," by P. S. Vanderkley.

---

*Prepared by W. L. Bradley

(ii) "Mode I Transverse Cracking in Epoxy and a Graphite/Epoxy Composite," by D. R. Williams.

2.2 Experimental Procedure

Two types of specimens have been employed in this work; namely, compact tension specimens (CT) and double cantilever beam specimens (DCB), as shown in Figures 1 and 2, respectively. Panels of Hercules 3502, 12" x 6" x 0.1", have been made with and without AS1 carbon fibers. The slot with the crack starting notch was made parallel to the fibers for the CT specimens cut from the panel containing unidirectional fibers. Thus, the crack path was transverse to the loading direction but parallel to the fiber direction; i.e., as in transverse cracking in a 90° specimen. The CT specimens of neat material and graphite/epoxy were precracked by gently tapping a razor blade placed at the root of the machined-in notch, inducing a natural crack to form.

Similar graphite/epoxy panels 12" x 6" x 0.1" were prepared with a strip of teflon placed along one edge at the midthickness. Subsequently, 1" x 12" x 0.1" DCB specimens were cut from these panels with the teflon tape serving as a crack starter at one end. When these specimens are loaded symmetrically, pure Mode I delamination results. However, when they are asymmetrically loaded, a combined mixed mode I/II fracture results, as shown in Figure 3.

It should be noted that the transverse cracking in the CT specimen is not identical to the delamination cracking in the DCB specimen, though both pass principally through the matrix. The delamination cracking occurs through a resin rich region which occurs between layers and is typically 1 to 2 fiber diameters in thickness. The transverse cracking parallel to the fibers occurs through whatever resin is available in the respective

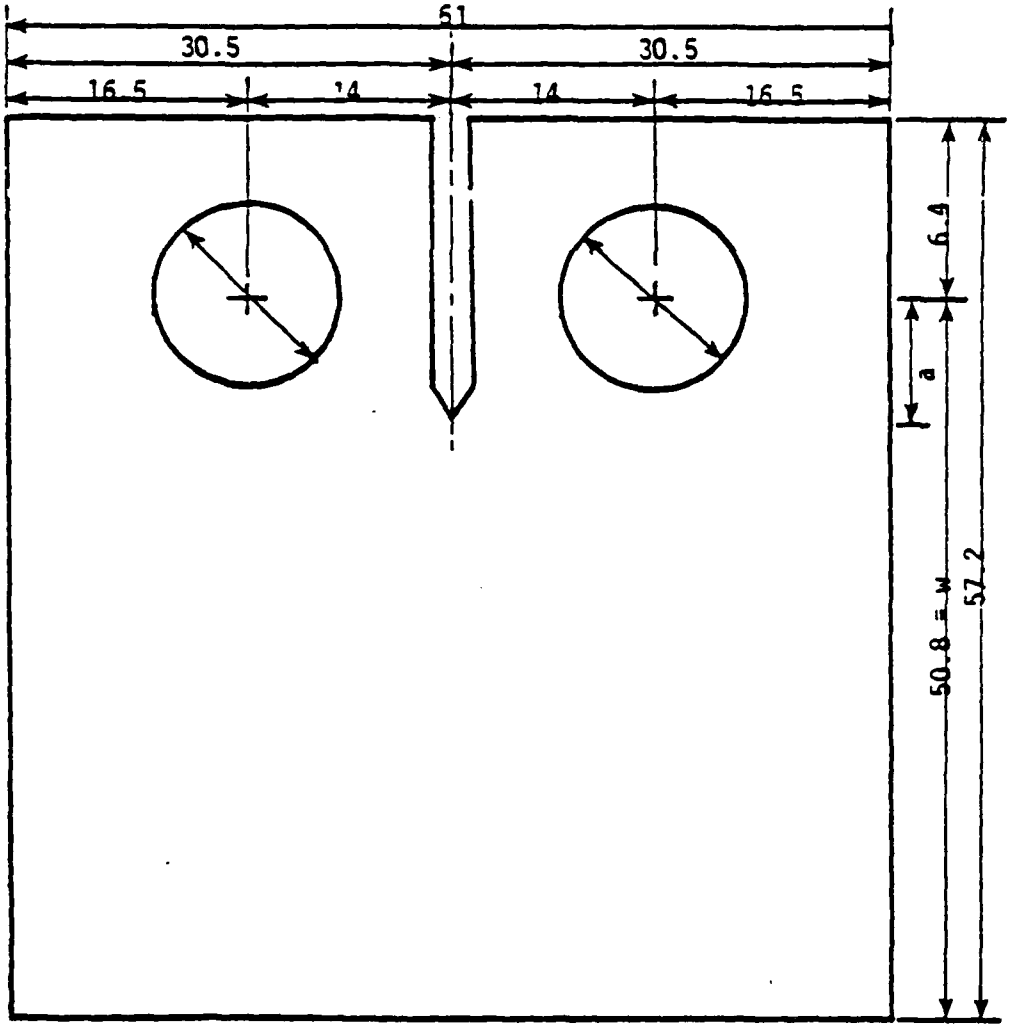

Figure 1. Scale drawing of compact tension specimens used in this study, with dimensions in mm.

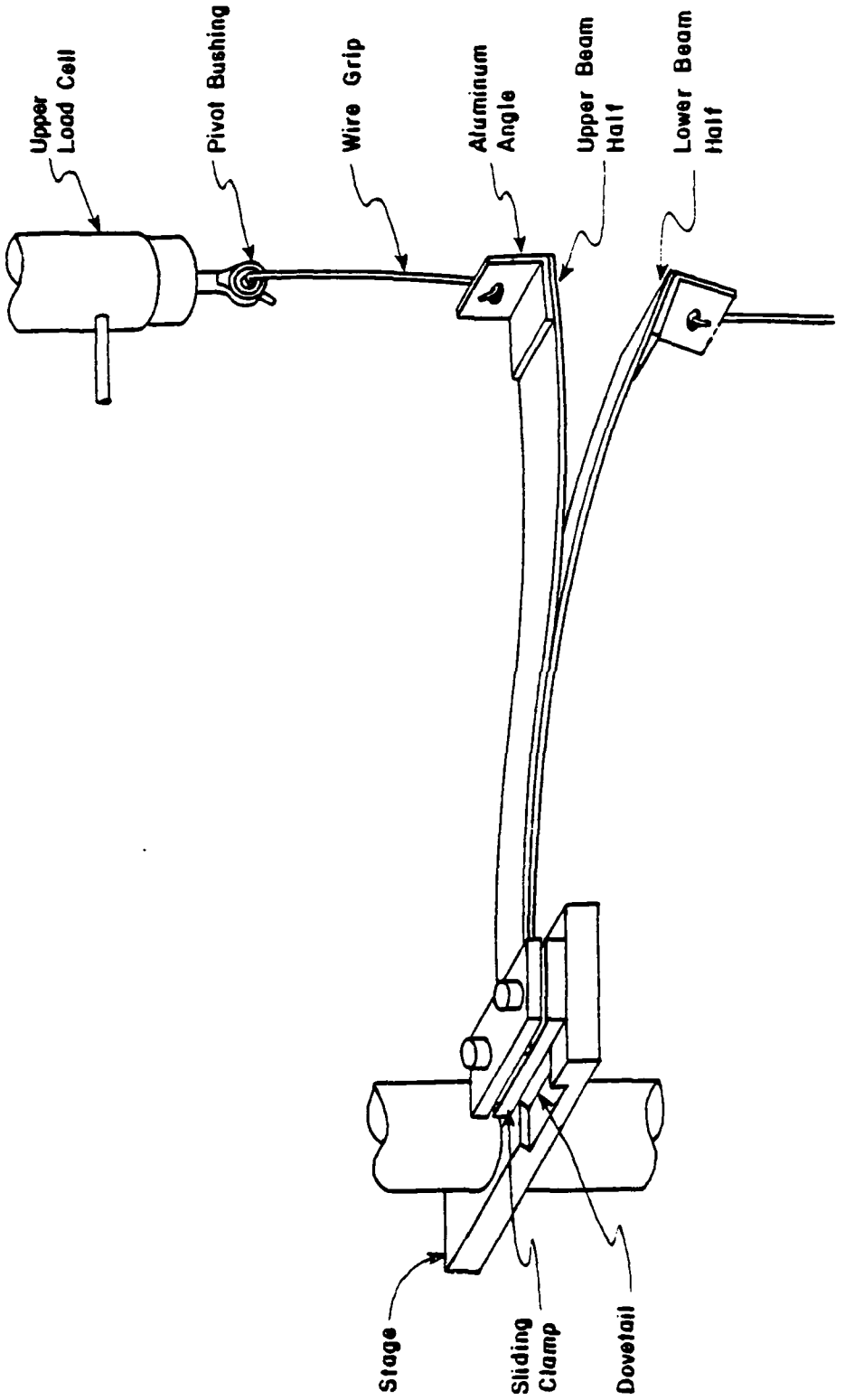

Figure 2. Stage, specimen, and grip configuration

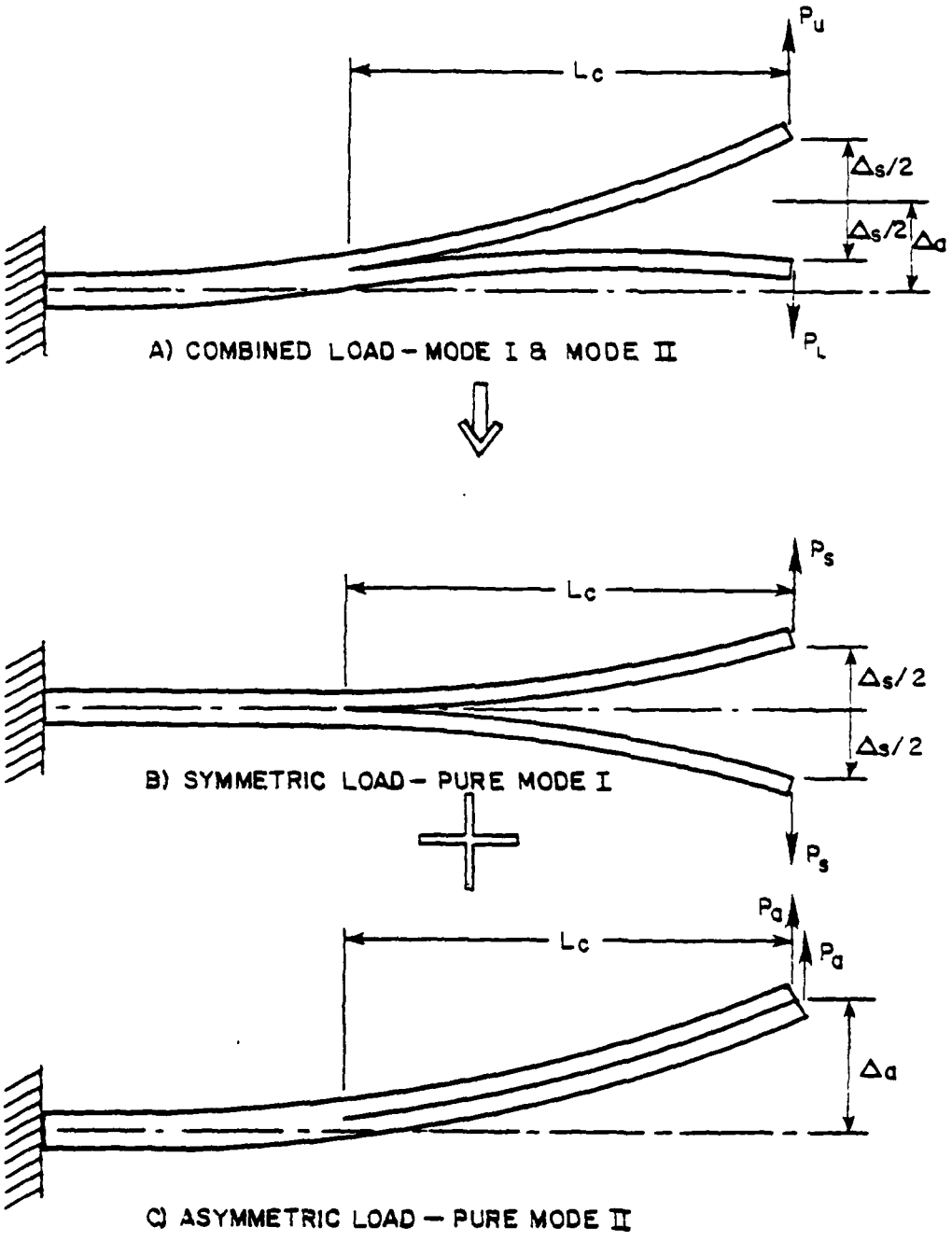

Figure 3. Superposition of a combined loaded beam into a symmetric (pure mode I), and an asymmetric (pure mode II) case

plies, though this is considerably less than that available locally between plies for the usual method of processing laminates. This difference will be seen to significantly affect the fracture toughness results for matrix cracking.

2.3 Analysis of Experimental Results

The experimental results for the asymmetrically loaded DCB specimens have been analyzed using linear elastic fracture mechanics coupled with linear beam theory, which gives [2]:

$$G_I = \frac{8P_s^2 L_c^2}{BEI} \qquad G_{II} = \frac{6P_a^2 L_c^2}{BEI} \tag{2.1}$$

where B is the DCB width, EI is the stiffness of the beam section that is not yet cracked, L_c is the crack length in the DCB, P_s is the symmetric load, $\frac{P_u + P_L}{2}$, and P_a is the asymmetric load, $\frac{P_u - P_L}{2}$, where P_u and P_L are the upper and lower loads as seen in Figure 3. The total energy release rate is $(G_I + G_{II})$. Note that when the loading is symmetric (i.e., $P_u = P_L$) $P_a = 0$ and $G_{II} = 0$.

The critical energy release rate was determined in two ways from the compact tension specimens. First, compliance measurements were made for specimens with various relative crack lengths, a/w, and then the critical load to fracture the specimen was determined. The critical energy release rate was found using the relationship [3]

$$G_{1c} = \frac{P_Q^2}{2B} \frac{\partial C}{\partial a} \tag{2.2}$$

where P_Q is the critical load, B is the thickness of the compact tension specimen and C is the specimen compliance (δ/P), where δ = the total load

line displacement and P is the applied load.

The second method of determining the critical energy release rate from the CT specimens was indirectly through a determination of the critical stress intensity factor, K_{1c}. This was done using relationships for K_{1c} as a function of P_Q and (a/w) by Srawley [4] for isotropic materials and Mandell et al. [5] for othotropic materials. The two approaches give very consistent results.

Finally, the critical stress intensities were converted into critical energy release rates in the usual way with [3]

$$G_{1c} = \frac{K_{1c}^2(1 - \nu^2)}{E^*} \tag{2.3}$$

where E* for the isotropic neat material is the Young's modulus E, and for the orthotropic material is calculated from a compliance tensor using the relationship for effective modulus [6]:

$$\frac{E^*}{1 - \nu^2} = \left[\frac{b_{11}b_{22}}{2}\right]^{-1/2} \left[\left(\frac{b_{22}}{b_{11}}\right)^{1/2} + \frac{2b_{12} + b_{66}}{2b_{11}}\right]^{-1/2} . \tag{2.4}$$

Material constants from Tsai and Hahn [7] for AS1/3501 (which is very similar to AS1/3502) were used to evaluate $E^*/(1 - \nu^2)$.

2.4 Experimental Results and Discussion

The critical energy release rate results for pure mode I cracking may be summarized as follows:

A. neat material $G_{1c} = 69$ N-m/m^2

B. delamination cracking parallel to fibers $G_{1c} = 150$ N-m/m^2

C. transverse cracking $G_{1c} = 225$ N-m/m^2

These results clearly indicate that the presence of fibers in a brittle matrix enhances the toughness in a significant way. Earlier results by Bascom et al.[8] show that fiber reinforcement in a ductile matrix decreased the delamination toughness. These different effects can be rationalized in the following way. The deformation or damage zone ahead of the crack tip in a ductile or tough material involves a significant volume of highly deformed material, contributing to the energy dissipation that accompanies fracture. Fiber reinforcement seems to reduce the size of this "plastic" zone, giving a net decrease in the fracture toughness.

In a weak, brittle material, reinforcement by strong brittle fibers enhances the toughness. The "plastic" zone in epoxy 3502 is negligibly small, so that there is no reduction in "plastic" zone size associated with the introduction of fibers. However, where cracking occurs through a thin layer of resin bounded by fibers with even a modest amount of waviness, some interaction of the crack tip with the fibers is unavoidable. If the fibers are much stronger than the matrix, as they are for graphite/epoxy systems, then this interaction makes crack extension more difficult. Where this occurs, either fiber breakage or multiple initiation results, the latter giving rise to a scalloped appearance of the epoxy on the fractured surface. The greater G_{1c} for transverse cracking as compared to delamination (225 N/m vs 150 N/m) could be interpreted as resulting from the thinner layer of resin through which the cracking occurs, which results in more frequent interaction with the fibers.

For mixed mode delamination, typical results are seen in Fig. 4. These results indicate that increasing mode II loading increases the total energy release rate required for fracture. The shear stress acting on the delamination plane causes the plane of the maximum normal stress σ_1 to be-

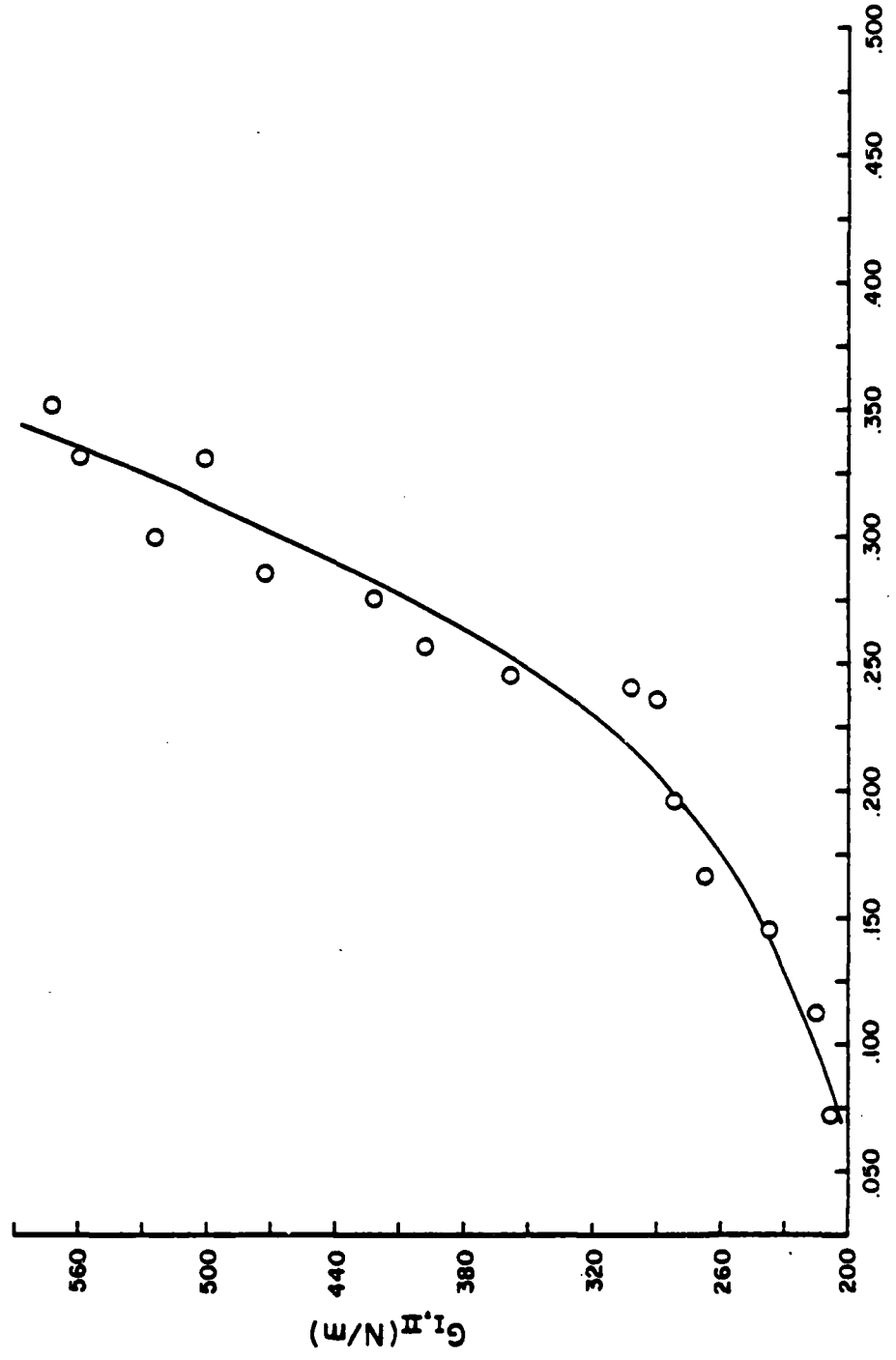

Figure 4. Total energy release rate ($G_{I,II} = G_I + G_{II}$) versus fracture of mode II energy release rate $G_{II}/(G_I + G_{II})$ for mixed mode delamination of graphite/epoxy composite (AS1/3502).

rotated relative to the plane of the lamina, the magnitude of this rotation increasing with increasing mode II shear. Crack extension in the brittle epoxy apparently will seek to follow the maximum normal stress plane. However, cracking in this direction may only proceed a short distance before the crack path is interrupted by the presence of fibers. Again either fiber breakage or multiple crack initiation results, giving a scalloped fracture surface [9]. The increasing $G_{I,IIc}$ with increasing mode II shear is the result of the crack continually being redirected into the fibers. While macroscopically we may say the fracture is mixed mode, microscopically the fracture behavior is probably that of a whole series of short pure mode I fractures on the maximum normal stress plane with tearing to coalesce these cracks, giving a crack path that in two dimensions looks like a saw blade for a handsaw. It is easy to see how increasing mode II changes the period of the scalloping, giving a greater total energy dissipation in fracture. The above micromechanistic model is strongly supported by fractographic observations made in a scanning electron microscope as presented in the theses of Vanderkley [2] and Williams [9].

In summary, matrix dominated cracking is greatly influenced by the presence of fibers, the greater the crack tip interaction with the fibers, the greater the toughness. Thinner resin rich regions and/or mode II shear serve to enhance this interaction, requiring larger values of energy release rate for crack extension. It should be noted the above generalizations are strictly applicable to a brittle matrix reinforced with stronger, brittle fibers. Different behavior would be expected for a composite with a ductile matrix.

3. MATRIX CONTROLLED FRACTURE ANALYSIS OF FIBROUS COMPOSITES*

3.1 Introduction

Experimental results described in Section 2 and in earlier reports on this project [1, 10] are helping to provide the basis for development of theoretical models of damage growth and fracture of polymeric composite materials. In this section we discuss additional experimental work and theoretical models which are concerned with the same objective. The following three M.S. Theses, whose Abstracts are collected in Section 7, cover a large part of the work discussed in this section:

(i) "Compression Induced Delamination in a Unidirectional Graphite/Epoxy Composite," by J. W. Earley.

(ii) "Mode I Delamination of Unidirectional Graphite/Epoxy Composite under Complex Load Histories," by J. S. Cullen.

(iii) "Analysis of the Effect of Matrix Degradation on Fatigue Behavior of a Graphite/Epoxy Laminate," by R. T. Arenburg.

The next three subsections briefly discuss the theses in the order listed. The last subsection, 3.5, abstracts a recent report of work on this project which is concerned with a theory of crack growth in nonlinear viscoelastic media. Both nonlinear behavior and viscoelasticity have been taken into account so that the theory will be general enough to apply to damage growth and fracture of composites exposed to a wide range of service environments over extended periods of time.

3.2 Compression Induced Delamination

The objective of the experimental phase of this research was to

---

*Prepared by R. A. Schapery

use in-plane compressive loading to induce delamination in Mode I fracture. A beam-column specimen geometry was employed, as shown in Fig. 5.

All of the beams were fabricated from Hercules AS1-3502 graphite/epoxy. The standard 15.24 cm wide prepreg tape was cut into 30.48 cm lengths, and these plies were used to fabricate a twelve-ply unidirectional (0°) laminate. One strip of teflon film was placed at the midplane to create the initial delamination. The panels were press cured using a press which was automatically controlled by a microprocessor, programmed with temperature, pressure and vacuum profiles. The panels were cut into 2.54 cm by 30.48 cm strips and side and end fittings were attached to each specimen. After the fittings were attached, the column was pre-cracked to assure an initial symmetric crack and to alleviate any artificial effects arising from the method of inducing the delamination.

Two other specimens were fabricated to determine independently the critical energy release rate from laminated beams split at one end; cf. Fig. 3B and [11]. The beams were fabricated by cutting the beam columns in half.

A constant side loading P_s, indicated in Fig. 5, was applied and then the beam column was compressed in an Instron test machine using a constant crosshead rate of 2×10^{-4} cm/sec. The specimens were tested in a dry state at room temperature.

The side loading provided a well-defined out-of-plane deflection and served to stabilize the beam against global buckling. We wanted to check the basic theory with a minimum of extraneous specimen-related factors; therefore, it was decided to introduce out-of-plane deflections

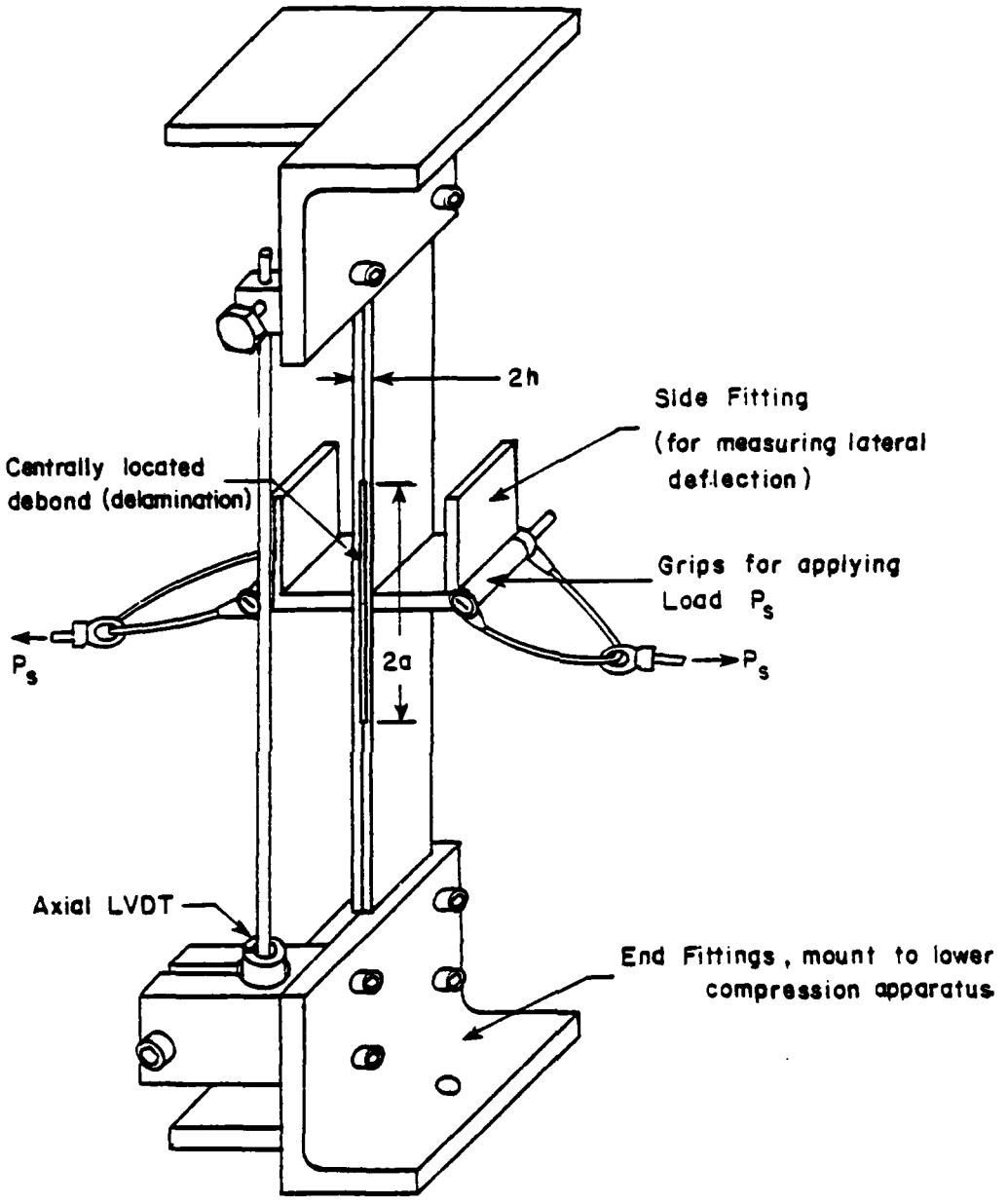

Figure 5. Test Specimen

in this manner instead of depending on (random) effects of initial imperfections such as slight initial beam curvature and load misalignment.

Figures 6 and 7 show typical results for axial deflection and energy release rate; the latter was predicted after using lateral displacement measurements to calculate crack length. The theory utilized the assumptions of classical beam theory and accounted for the geometric nonlinearity due to large rotations.

Primary conclusions reached from the study by J. W. Earley are:

1) For AS1-3502 graphite/epoxy in a dry state at room temperature, classical beam-column analysis linked with linear elastic fracture mechanics is applicable for determining axial and lateral deflections, strain energy, and energy release rate. (Similar agreement for more complex geometries has been reported by others [12].)

2) The average critical energy release rate obtained from beam-columns was 137 N-m/m^2 (.78 in-lb/in^2), which is close to the value of 127 N-m/m^2 found from end-split laminates.

3) The energy release rate during crack progagation was fairly constant throughout each test.

4) Increased lateral load did not have any significant effect on energy release rate, although it did increase the average crack speed.

5) The overall fracture path generally propagated through the resin between fibers, although failure along the interface with some fiber breakage was not uncommon.

6) Hackles, overlapping platelets of epoxy, and cleavage-like micro-cracks which branch near fiber epoxy boundaries were observed. These features could be used to determine the direction of damage progression in composite specimens.

3.3 Delamination Under Complex Load Histories

The specimen design chosen for this study was a twelve ply 2.54 cm x 25.4 cm (1 in x 10 in) Hercules AS1/3502 graphite/epoxy coupon speci-

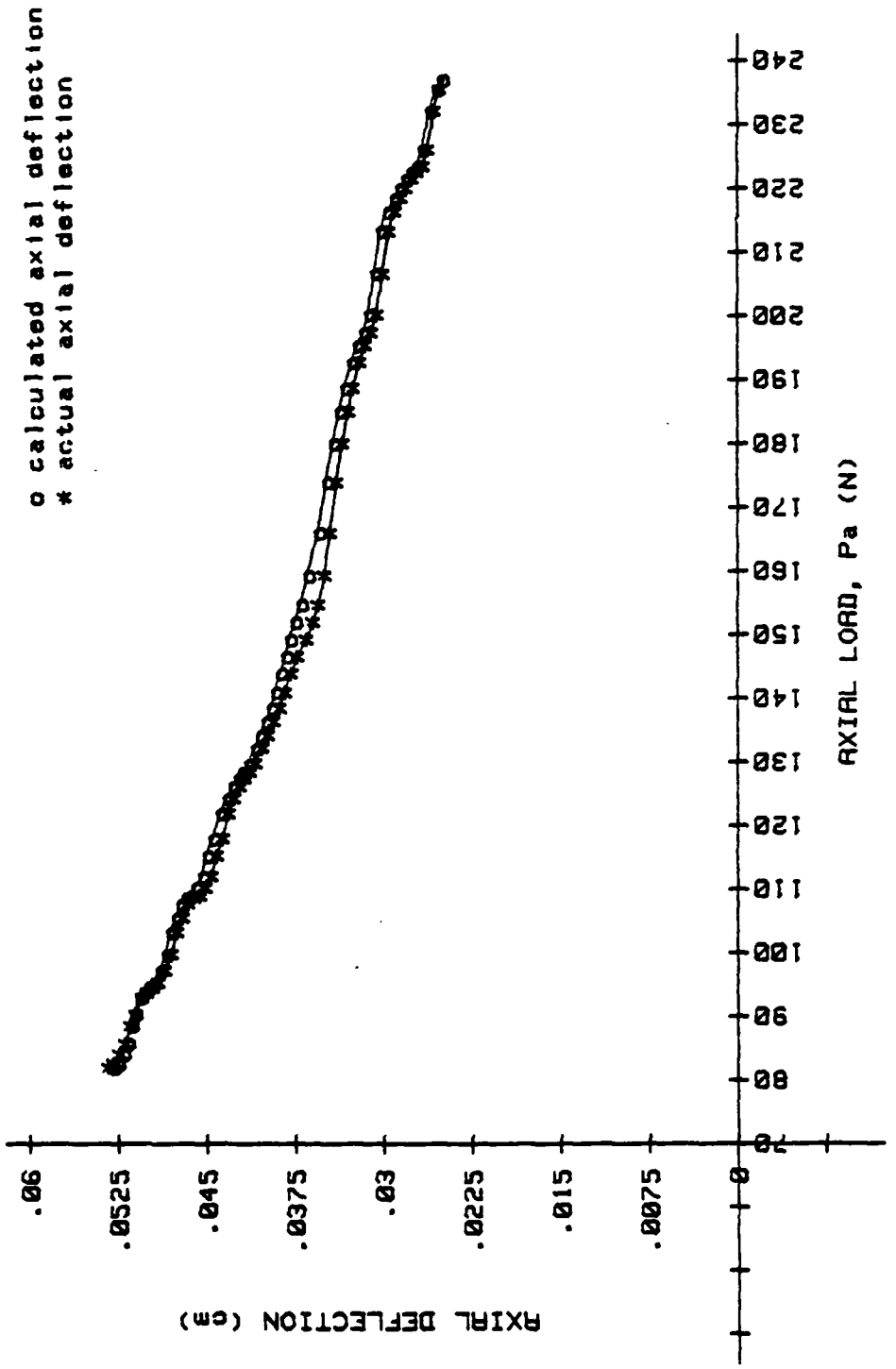

Figure 6. Axial Deflection vs. Axial Load for Specimen 43 (crack propagation portion only, test direction right to left).

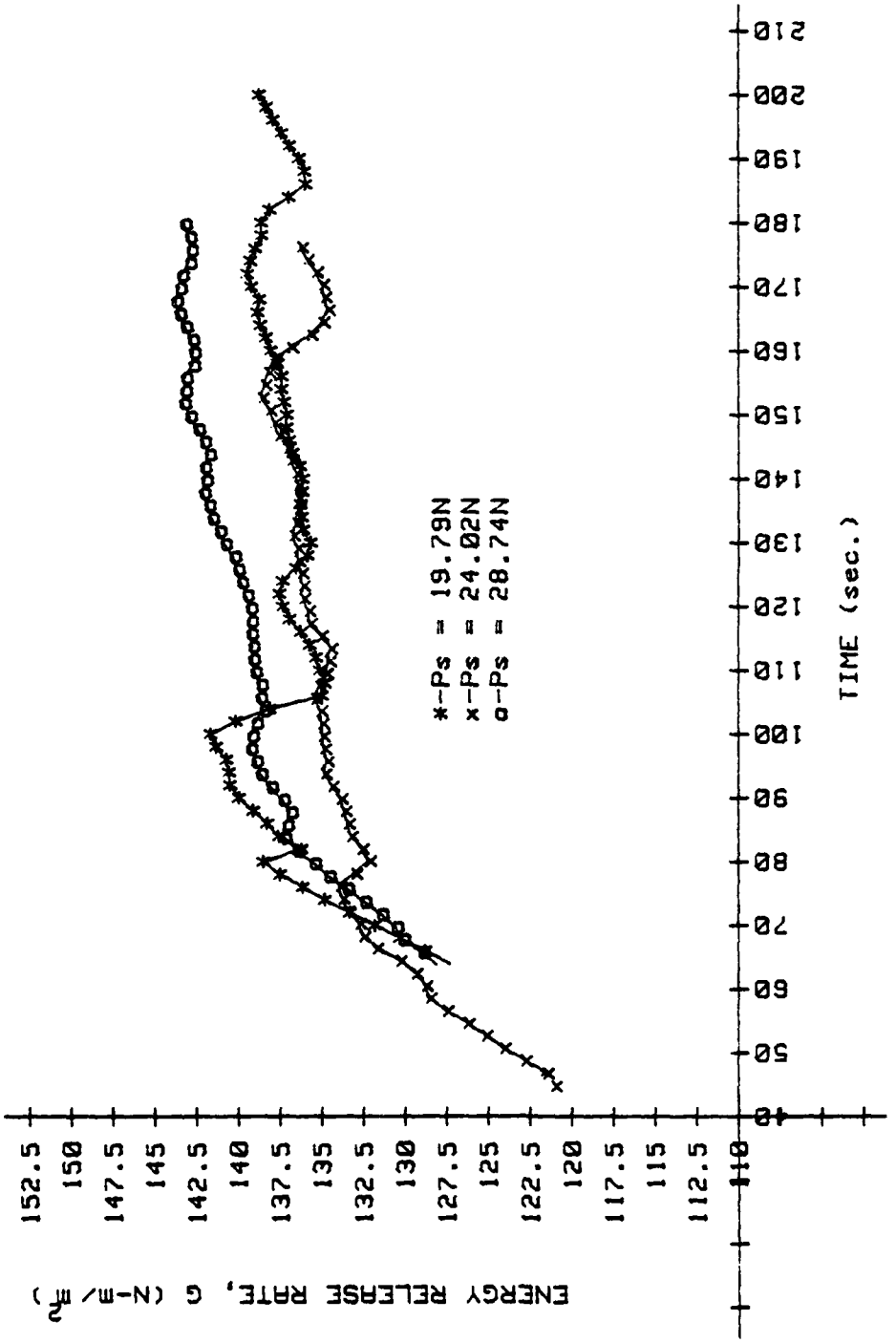

Figure 7. Energy Release Rate vs. Time for Specimens 37(*), 43(0), and 45(x).

men with fibers parallel to the beam axis. During lay-up, teflon was inserted at the mid-plane of the laminate at one end of the specimen to provide an initial delamination crack. Aluminum tabs were bonded to the same end in order to load the samples as shown in Fig. 3B; the left end of the beam was unsupported in these tests. For the elevated temperature/humidity testing, the desired moisture content was obtained by placing specimens in an environmental chamber at a humidity of 95% RH and temperature of 70°C. The constant humidity was maintained by a saturated solution of potassium sulfate in the bottom of the closed chamber. Equilibrium moisture content was obtained by conditioning the samples for six weeks prior to testing.

The specimens were tested at ambient (55% RH, 23.9°C) and elevated (95% RH, 93.3°C) environments under the transient and cyclic crack opening displacements (COD) Δ (Δ_s in Fig. 3B) illustrated in Figs. 8 and 9. An MTS servohydraulic testing machine interfaced with a Digital Equipment MINC-11 data acquisition laboratory computer system was used for the experiments. An environmental chamber maintained the desired conditions during testing.

Figure 10 shows typical cyclic test data; crack growth occurs along the upper load curve, which decreases with increasing displacement. Observe that upon reloading, a larger load is needed to initiate crack growth than existed at the start of unloading. Crack growth was not continuous along the upper curve, but instead propagated in a stop-start fashion. This stop-start behavior also existed in the constant displacement rate tests, as may be seen in Fig. 11. This type of unstable crack growth has been reported by others in studies of resin fracture [13-15].

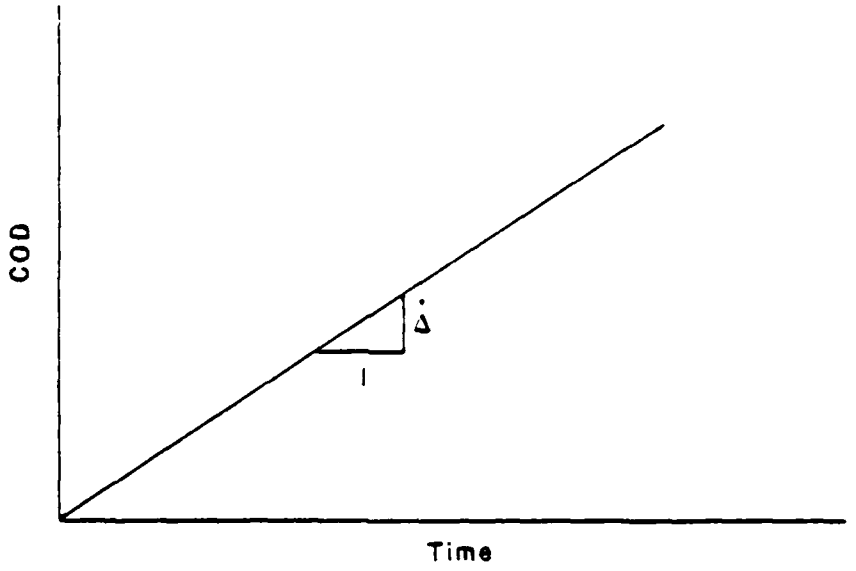

Figure 8. Constant Displacement Rate Loading History.

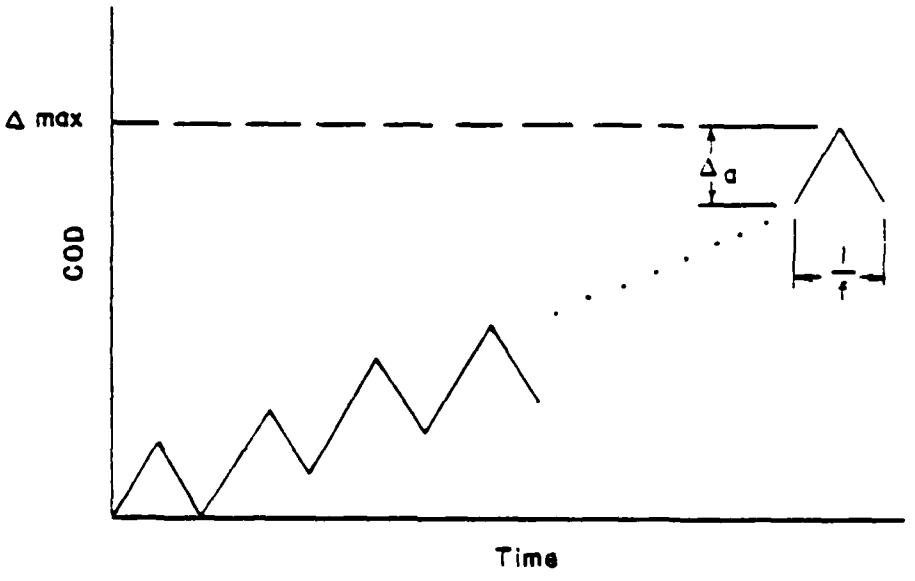

Figure 9. Cyclic Loading Histories (5 and 25 Cycles).

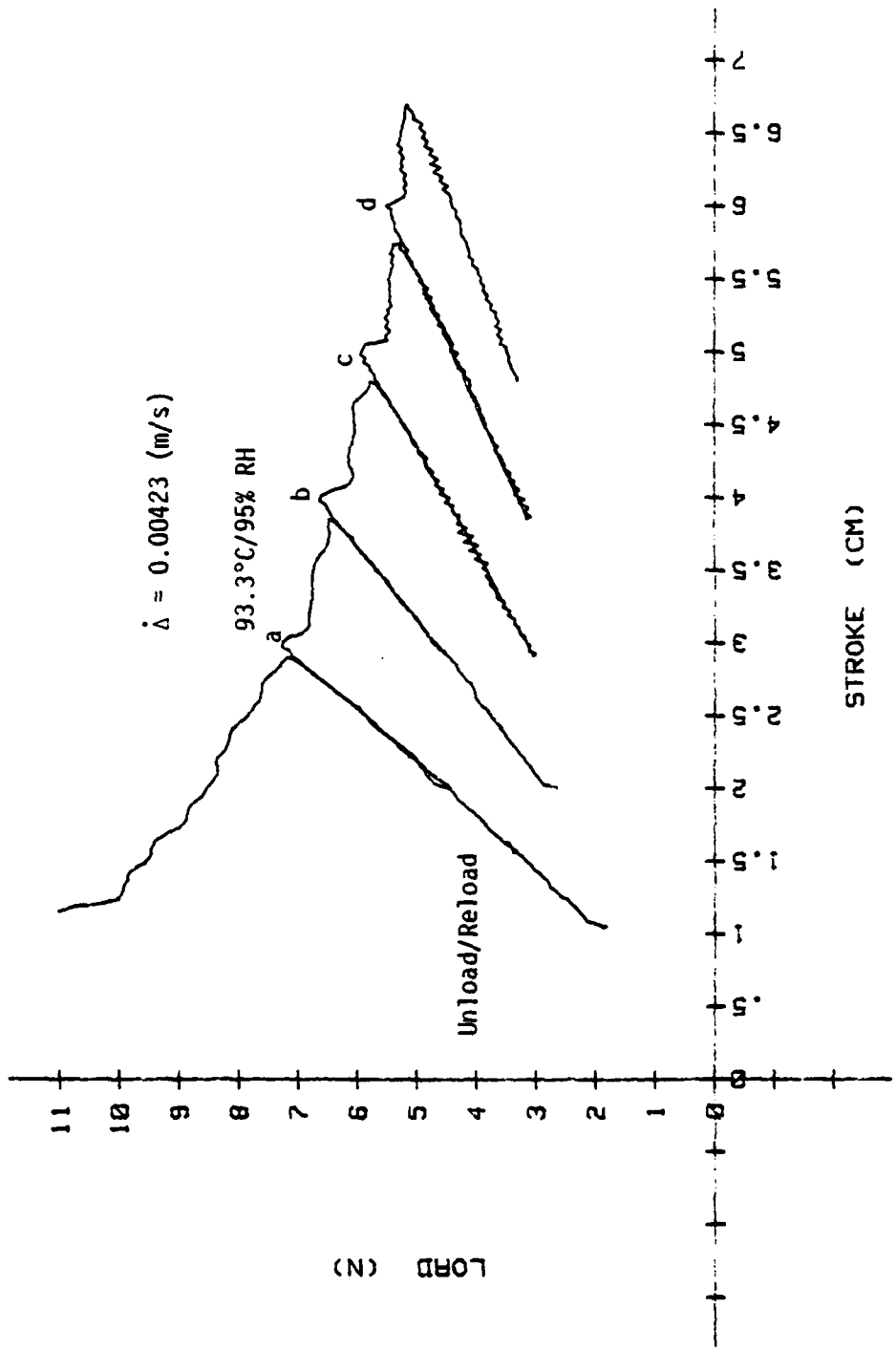

Figure 10. Load vs. Crosshead Displacement for a 5 Cycle Test (Specimen 28).

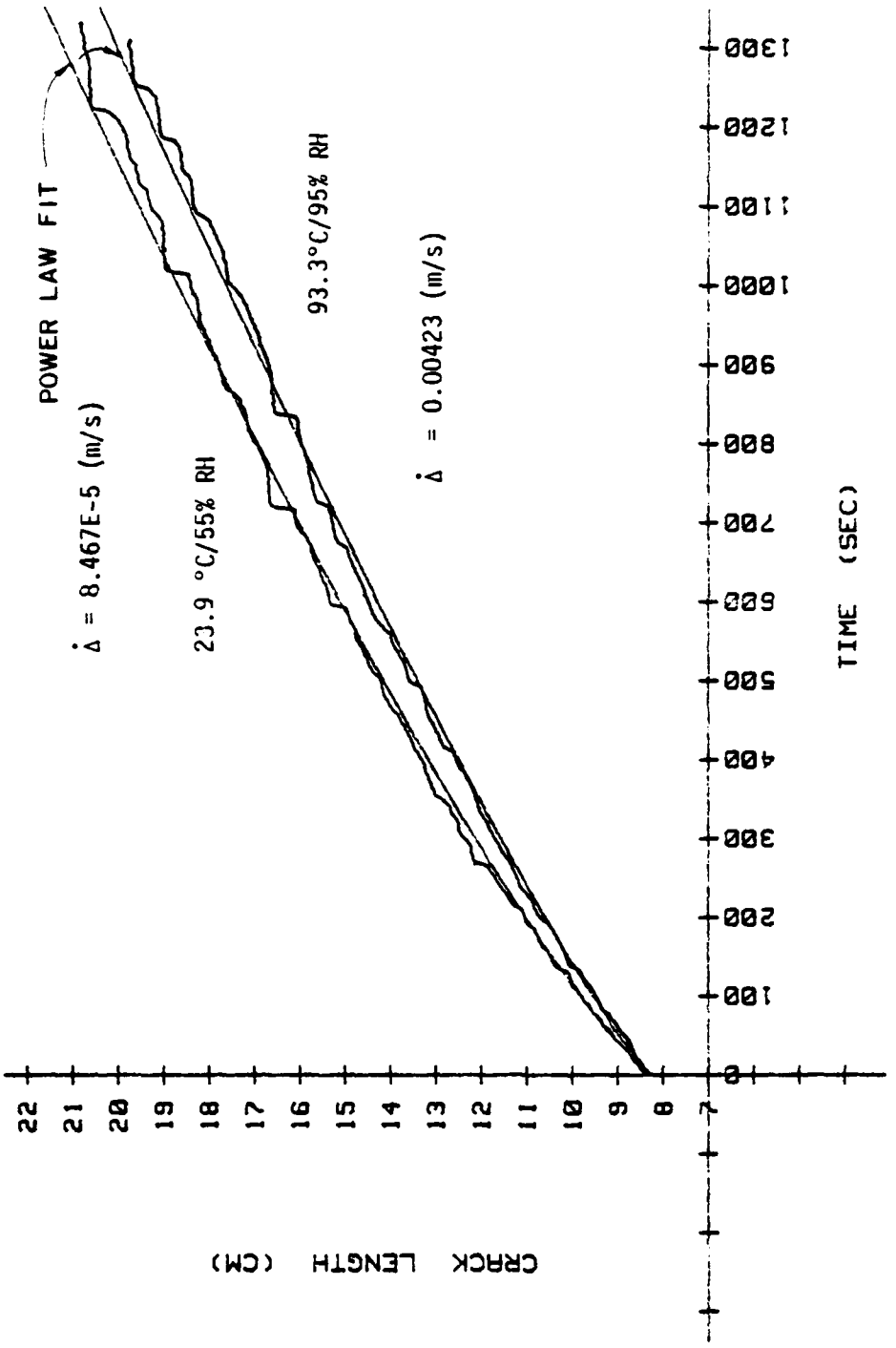

Figure 11. Crack Length vs. Time for a Ramp Test (Specimen 25, 93.3°C and Specimen 6, 23.3°C).

A quasi-static viscoelastic analysis reported last year [1] predicted a curve of G versus crack speed $\dot{a}$ which has a negative slope except at very low speeds. Figure 12 illustrates such a curve, which may help to explain the observed unstable crack growth. When G exceeds the value required for growth at point "a", G_{1q}, the crack propagates dynamically. However, for quite slowly applied displacements, the available G decreases rapidly until it reaches the value G_{1a}, the "arrest energy". Unless the applied load is removed, the crack does not truly arrest in this model, but rather has the speed at point "d". The proposed G vs $\dot{a}$ behavior is indicated by the arrows in Figure 12, and is typical of the behavior found from all of the tests; Figure 13 shows such behavior.

Further analysis of the data is needed to determine if the crack actually stops propagating during this cycle of "stop-start" propagation, or if it just slows to the point "d" in Fig. 12 before repeating the cycle. A more detailed study will have important implications for the understanding of crack tip deformation processes and development of crack growth theory. A theory based on cycles of true initiation and arrest will be quite different (in detail, at least) than a theory based on continuous, but uneven, growth.

General conclusions that may be drawn from J. S. Cullen's thesis are:

1) The maximum ("initiation") energy G_{1q} increases with increasing temperature and moisture and decreasing applied displacement rates.

2) The stop-start type of unstable crack growth is most apparent at the highest temperature and moisture levels.

3) The minimum ("arrest") energy is approximately 90% of G_{1q} for the composite materials and test conditions employed. (Differences

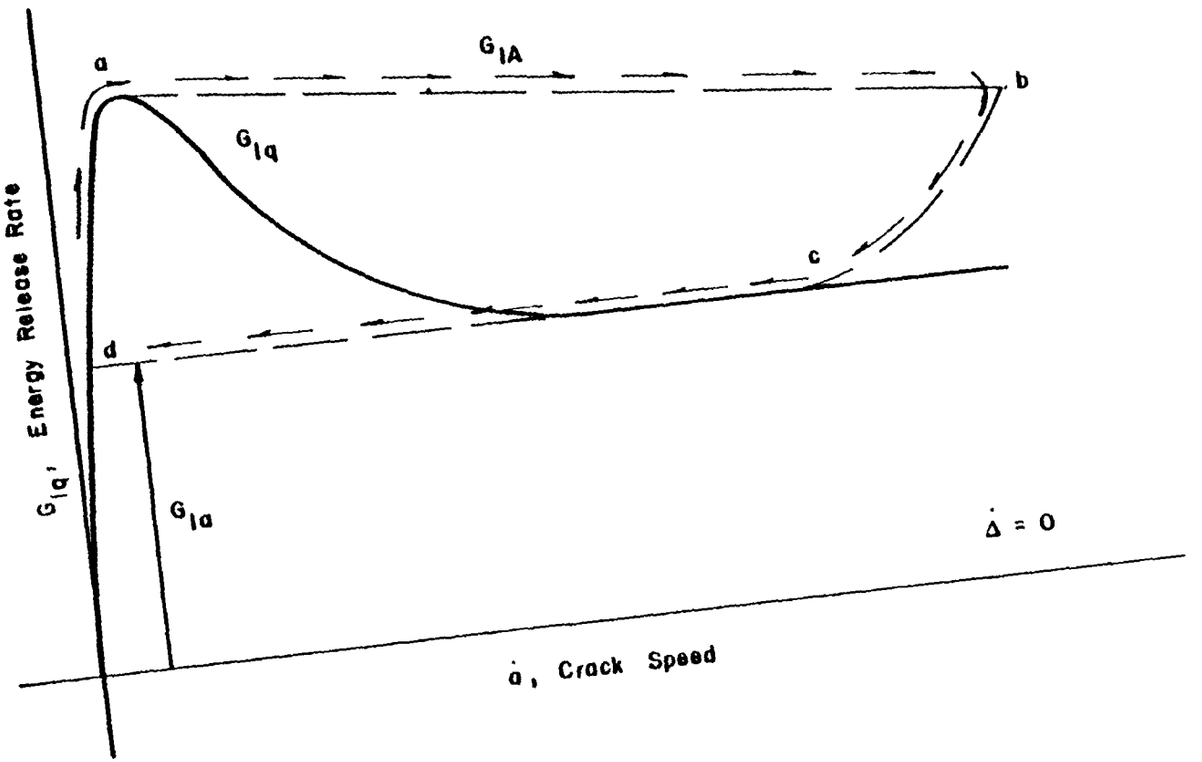

Figure 12. Hypothesized Relationship Between Energy Release Rate and Crack Speed.

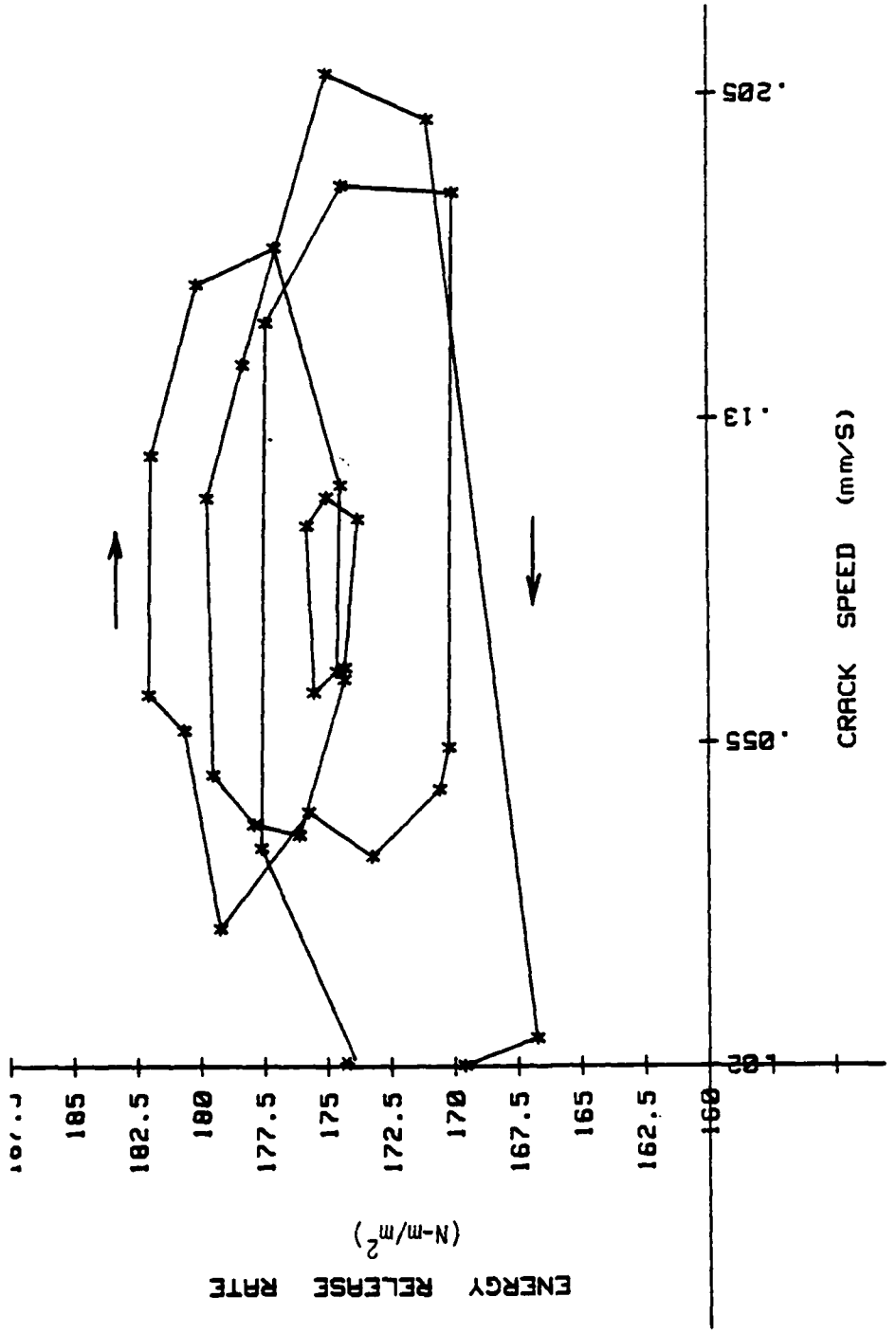

Figure 13. Energy Release Rate vs. Crack Speed Showing Local Unstable Crack Growth ($dG/da < 0$).

between initiation and arrest values for resins may be much larger [13-15].

3.4 Analysis of Effect of Matrix Degradation on Deformation and Strength

Tensile failure of laminates is often a direct result of delamination which initiates at free edges, such as illustrated in Figure 14. R. T. Arenburg's thesis is concerned with the prediction of the mechanical state and energy release rate for delamination in tensile coupons with various amounts of delamination and matrix degradation (e.g., due to microcracking). A detailed study of a $[\pm 45/90_2]_s$ graphite/epoxy laminate was made using theory developed in the thesis and experimental data reported elsewhere [16]. Guided by both theory and experiment, symmetrical delaminations between the 45° and 90° plies were assumed to be the primary macroscopic cracks, and therefore energy release rate in only this mode of fracture was analyzed.

Figure 15 shows the effect of reduced values of the resin's Young's modulus E^m on the predicted axial modulus E_{LAM} of the laminate; E_{REF} is the latter modulus based on the unreduced matrix modulus $E^m_{initial}$. Experimental values of the axial mean strain significantly increased during fatigue loading at constant load amplitude and R-value [16]; typical behavior is sketched in Fig. 16, in which the rapid increase in strain near failure is due to delamination. Viscoelastic effects without matrix damage were far too small to explain the strain increase (even well before the high strain rate period near failure) [16], and there was no significant amount of fiber failure until the final stages of fatigue failure. Therefore, prior to delamination the increase in strain was assumed to be due to matrix damage, idealized for purposes of theoretical analysis by a cycle and stress-dependent matrix modulus. Using the finite element

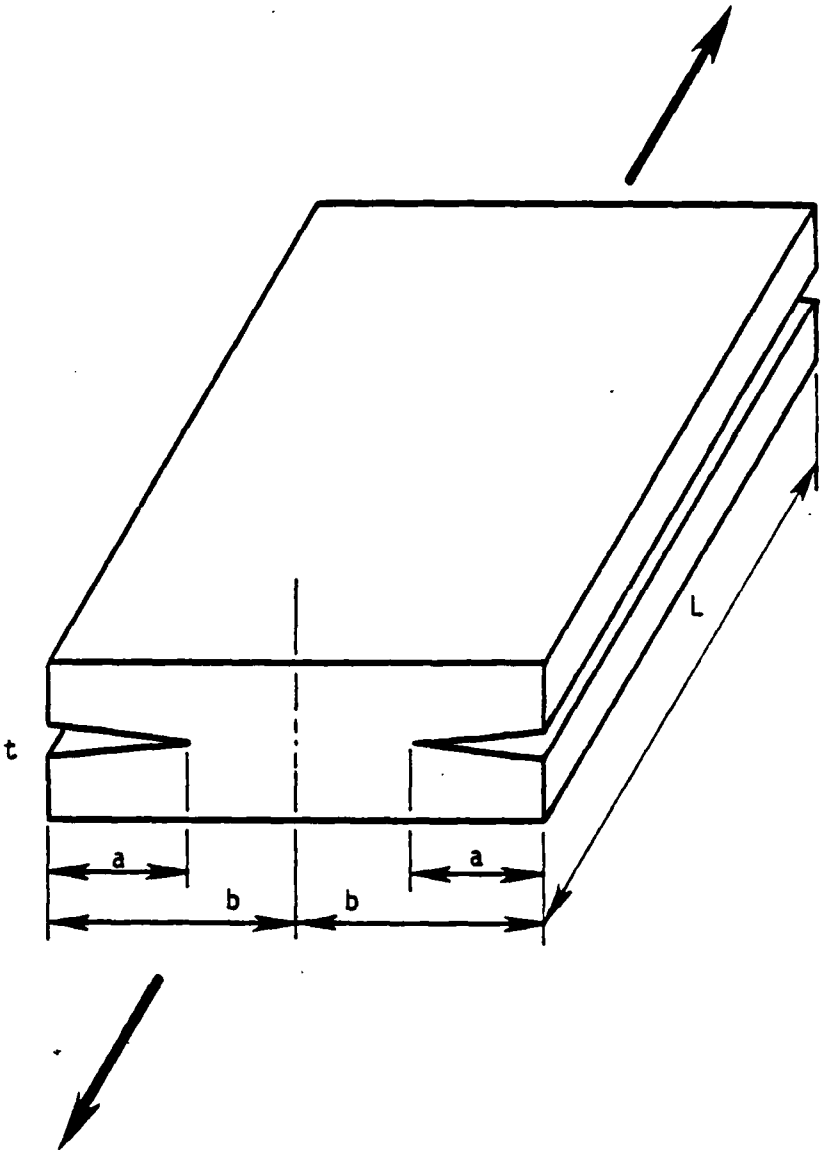

Figure 14. Configuration of delamination

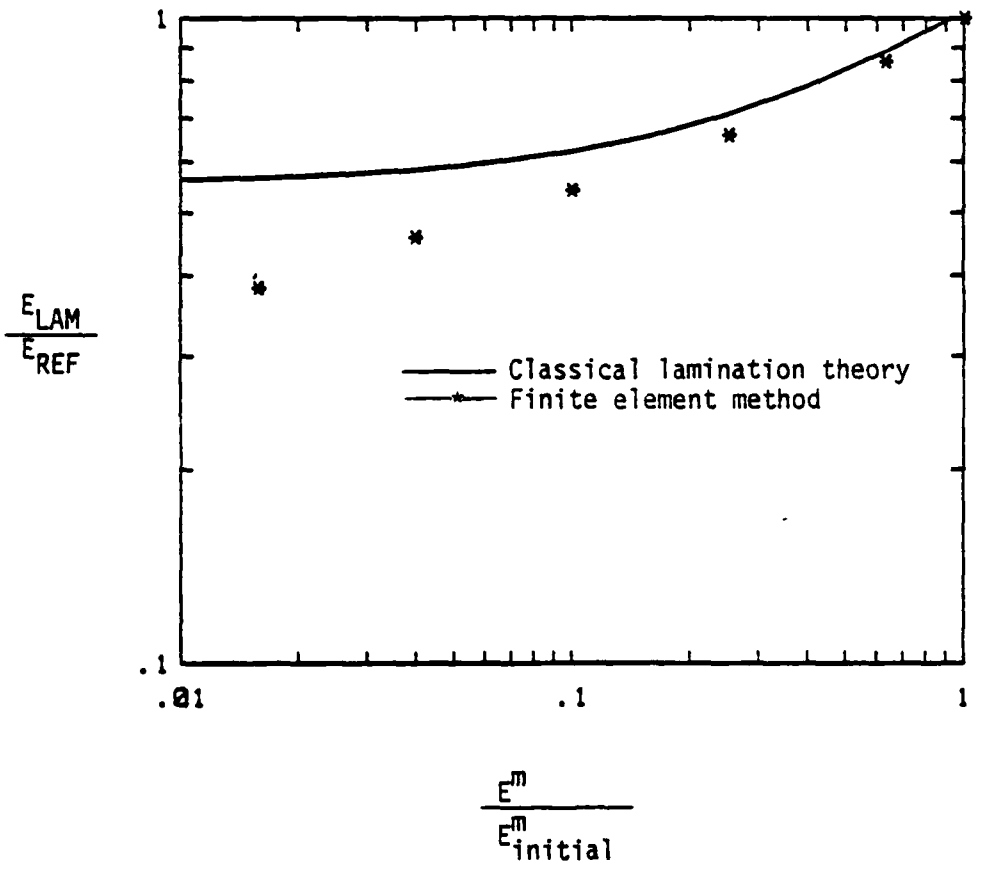

Figure 15. Axial laminate stiffness as a function of matrix modulus.

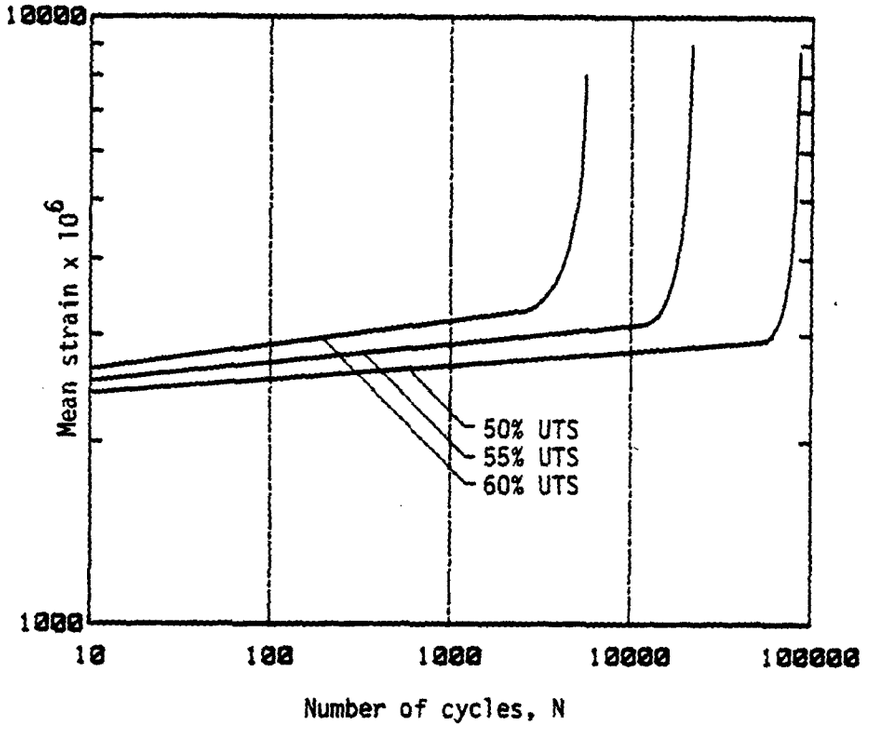

Figure 16. Idealized mean strain curves for a $[\pm 45/90_2]_s$ laminate.

results for modulus in Fig. 15 and the strain data in Fig. 16, it was estimated that $E^m/E^m_{initial}$ has to be in the range from 0.1 to 0.25 just before the rapid upturn in the strain curves if the predicted and experimental strains are to agree at this point; the largest amount of matrix damage near failure (ratio of 0.1) corresponds to the lowest stress (50% UTS).

Figure 17 gives the theoretical prediction of energy release rate as a function of crack length/ply thickness for three different values of matrix modulus; "O'Brien's method" is based on classical lamination theory. In order to test the proposed model of fatigue failure, a representative critical energy release rate of G_c = 175 N/m was used (along with the estimated amount of matrix degradation) to predict the initial flaw size that would result in unstable delamination; values close to the ply thickness were calculated, which is a very encouraging result. Furthermore, without matrix degradation, the energy release rate in Fig. 17 is far below that needed to cause unstable delamination, regardless of the size of the initial delamination, for the stress levels used in [16].

Several conclusions can be made from R. T. Arenburg's analysis:

1) Matrix degradation modeled by a reduced matrix modulus through micromechanics principles shows considerable promise as a means to analyze fatigue behavior. However, the study conducted was of a preliminary nature in that only mean stress and mean strain responses were considered, and the influence of stress gradients on matrix damage was neglected.

2) In evaluating laminate stiffness, it was found that as the matrix modulus was reduced, considerable shear deformations occurred which classical lamination theory was unable to model. The shear deformations, which are associated with free edge effects, were found to penetrate a considerable distance in from the free edge. For the smallest value of the matrix modulus, the finite element method showed that the free edge effects were extended five laminate thicknesses into the interior of a $[\pm 45/90_2]_s$ laminate.

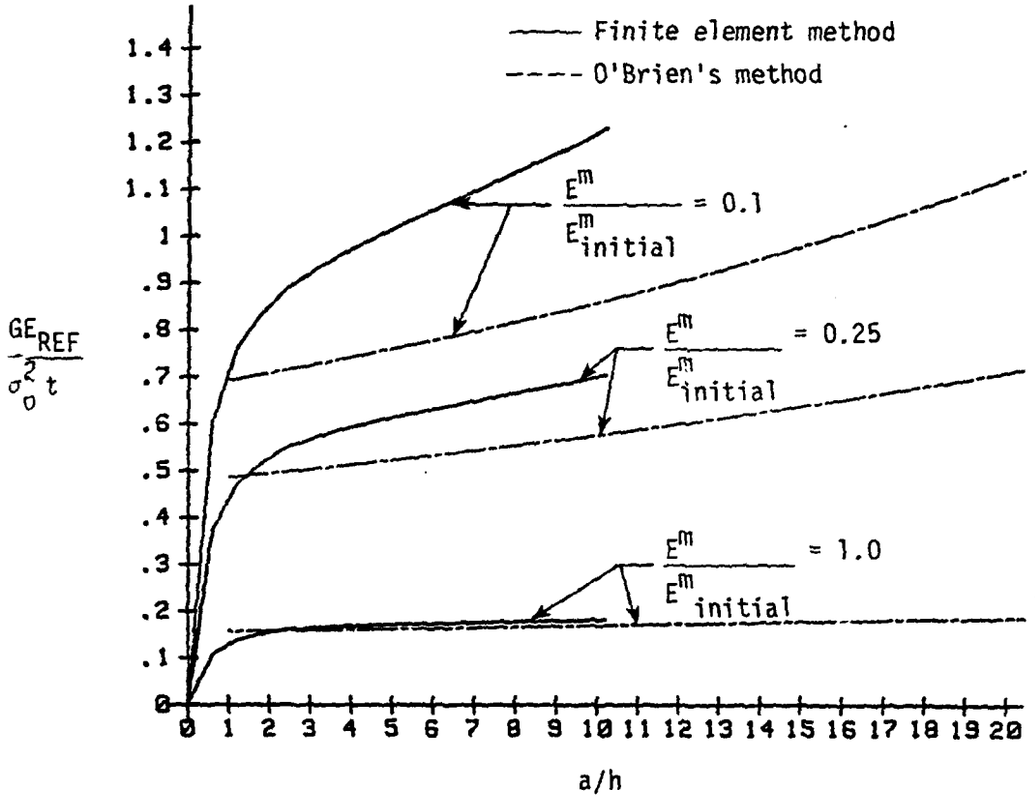

Figure 17. Total normalized strain energy release rate as a function of delamination length/ply thickness for a constant stress condition.

3) A parametric study of free edge delaminations as a function of matrix damage was performed for constant maximum strain and constant maximum stress fatigue tests. For the constant strain fatigue test the available energy for delamination was predicted to be greatest at the beginning of the test and then was subsequently reduced by the matrix damage. In a constant stress fatigue test, the effect of matrix damage was to increase the available energy for delamination. As illustrated in Fig. 18 for a laminate with constant critical energy release rate G_c, with sufficient matrix damage (decreasing matrix modulus) a crack of initial length a_o will become unstable.

3.5 Generalized Models for Damage Growth and Fracture

The preceding discussion illustrated the importance of accounting for distributed damage in the prediction of deformation and fracture of composites. Considerable extension beyond the use of a single parameter reflecting the damage, such as a uniform reduced matrix modulus, is necessary to achieve a sufficiently general theory for engineering uses. Microcracking (and other damage mechanisms) in general will be nonuniformly distributed, produce directional softening, and depend on histories of the mechanical and physical environments.

As an aid to understanding and prediction of complex damage phenomena, a viscoelastic crack growth theory for nonlinear media was recently developed on this project [17]. Starting with a nonlinear viscoelastic constitutive equation in the form of a modified superposition integral, correspondence principles are established in [17] which enable viscoelastic stresses and deformations to be easily predicted from a nonlinear elasticity solution; one correpsondence principle applies with stationary or growing cracks, while another may be used with time-dependent joining and healing of initially separate surfaces. The first of these correspondence principles leads to a generalized J-integral for use in predicting fracture initiation time and crack speed. An important step in this analysis is the derivation of nonlinear, non-singular solutions for

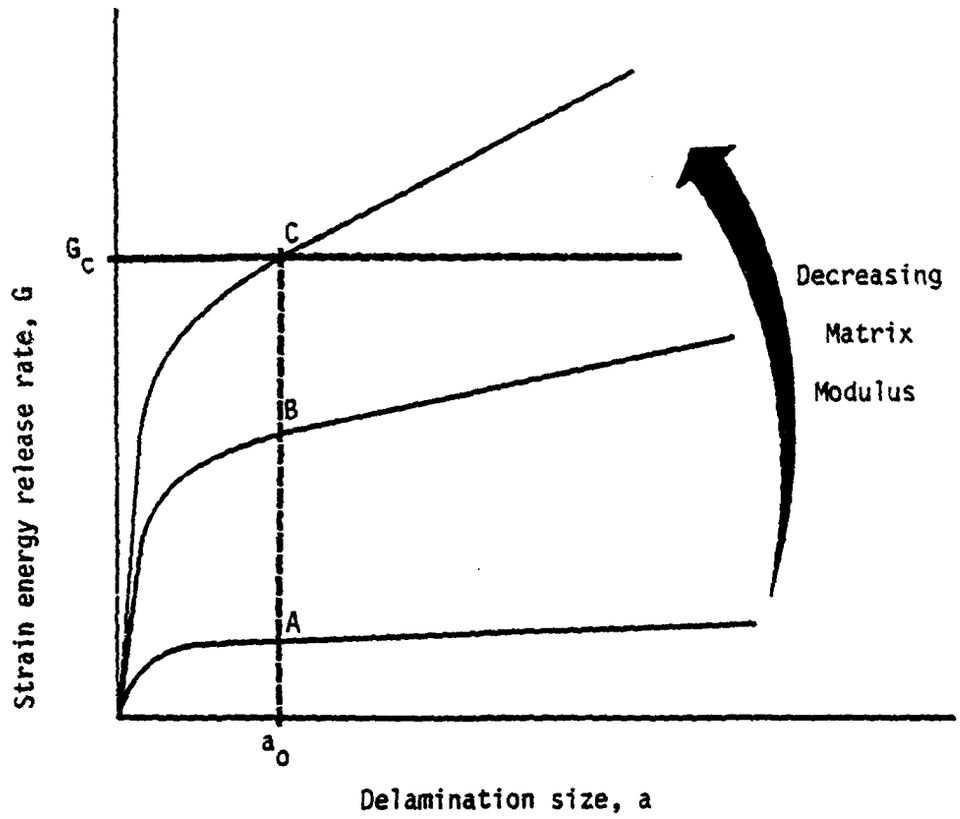

Figure 18. Delamination growth criterion for a constant maximum stress fatigue test.

the mechanical state of the neighborhood of the crack tip; singular solutions result in physically unacceptable viscoelastic fracture criteria. Several explicit results for the initiation and growth rate of cracks are obtained in [17] assuming the strain energy density for the associated elastic material is a homogeneous function of the strains (i.e. the stress is a power-law function of strain).

Results from this theory have been used in a study of the relation between crack speed and the J-integral [18], and in the development of damage models for composites with emphasis on effects of particle reinforcement [19].

Currently, we are working on extending the damage theory to laminates.

4. STRESS AND DEFORMATION ANALYSIS OF RESIN AND COMPOSITE MATERIALS*

4.1 Residual Stresses

An investigation of the effects of moisture and temperature on residual stresses in composite laminates is continuing. A major portion of the effort during the past year was conducted as part of a Ph.D. dissertation project "On the Effects of Post Cure Cool Down and Environmental Conditioning on Residual Stresses in Composite Laminates" by Mr. B. D. Harper.

Solution forms which relate curvatures in unsymmetric cross-ply laminates to temperature excursions and moisture content, including viscoelastic effects, were formulated and programmed. Progress was made concerning the specimen design, regarding both plates and beam-like coupons. The design strives to keep the thickness dimension small enough to ensure both measurable curvatures and reasonably short moisture saturation times. On the other hand it is desirable for deflections to be small enough to permit usage of linear beam and plate theory. Several lay-ups were considered with staggered 0° and 90° plies to avoid premature cracking due to residual stresses. The range of validity of the classical linear plate theory was examined by analyzing some different large deformation problems.

An improved device to measure curvatures was constructed and several environmental chambers were assembled. Also, as part of the dissertation project, preliminary work was done on the curing of bi-material coupons made of Hercules 3501-6 resin and aluminum backing in preparation for investigating cure-shrinkage effects in AS/3501-6 graphite/epoxy composites.

---

*Prepared by Y. Weitsman

Some earlier work on moisture effects is covered in the recent publication by Y. Weitsman, "A Rapidly Convergent Scheme to Compute Moisture Profiles in Composite Materials under Fluctuating Ambient Conditions," J. Composite Materials, Vol. 15 (July 1981), pp. 349-358. A reprint is included in Appendix A.

4.2 Optimization of Cooling Histories

A theoretical investigation was conducted on optimal cool-down paths for minimizing residual stresses in cross-ply laminates and adhesive joints. A report by Y. Weitsman and B. D. Harper, "Optimal Cooling of Cross-Ply Composite Laminates and Adhesive Joints," describes this work, and is included in Appendix A.

The investigation was based upon a previous formulation of the optimal cool-down idea, but extended the scheme to include the technically important case of temperature-dependent transverse and longitudinal coefficients of thermal expansion, α_T and α_L. Specific calculations were conducted for epoxy/aluminum joints and two kinds of graphite/epoxy composites using the best currently available data. It was noted that while the optimal time-temperature paths did not vary appreciably for temperature-dependent α_T and α_L, a further reduction was found in the residual stresses at the termination of cool-down when the specific variations of thermal expansion coefficients were considered.

4.3 Shear Deformation in Laminated Plates

An investigation of shear deformation effects is reported by Mr. B. A. Coulter in the M.S. thesis "Shear Deformation Effects in Composite Laminates". This investigation, which is abstracted in Section 7, includes a study of elastic effects in plates subjected to several types of normal

loadings; it was shown that sharp spatial variations of external loads may cause very significant shear effects, sufficient to invalidate the results of classical plate theory. Such departures from classical theory may occur even for thin laminates. In addition, a viscoelastic version of the shear deformation theory was employed to predict material damping due to the time-dependent response of the resin component. Again, it was found that under sharp spatial variations in external loadings, as well as for thick laminates, the classical plate theory may grossly under-predict the amount of material damping available due to the viscoelasticity of the resin.

4.4 Analysis of Crazing

An inquiry was initiated to represent damage growth in polymeric resins due to crazing prior to cracking. It appears that in moist environments crazes tend to extend and stretch under constant loads, a behavior that is probably attributable to the accentuated viscoelasticity of the crazed material which diminishes its load carrying capacity. On the other hand dry crazes ("air crazes") appear to grow by drawing additional material from the polymerized regions across sharply defined interfaces. In this case the energetics of the phenomenon must account for energy required to affect such phase transformation. The mechanics formulation of these behaviors requires the solution of some well-defined boundary value problems, which are currently being set-up.

5. VISCOELASTIC FINITE ELEMENT PROGRAM*

The nonlinear viscoelastic theory of Schapery [20] was examined in detail during 1979 and 1980 as a possible means of accounting for hereditary behavior within the context of an incremental, nonlinear finite element program. The integral equations were recast into incremental form and a time-marching, recursive numerical procedure was developed for evaluating certain time-dependent strain functions. During 1980 and 1981, this numerical procedure was incorporated into the nonlinear finite element program, AGGIE, in a general three-dimensional format. Several applications were made to uniaxial and biaxial creep problems and comparisons were made to experiment and other creep models. Results of some of these comparisons are reported [21, 22].

The viscoelastic constitutive model for isothermal conditions and infinitesmal strains is given by [20],

$$\varepsilon_{ab} = J(0)\sigma_{ab} + \frac{\partial \hat{\sigma}_{cd}}{\partial \sigma_{ab}} \int_{-\infty}^{\psi} \Delta J(\psi - \psi') \frac{dG_{cd}}{d\psi'} d\psi' \tag{5.1}$$

$$\psi = \int_{0}^{t} \frac{a_G}{a_D} dt, \tag{5.2a}$$

$$G_{cd} = \frac{\hat{\sigma}_{cd}}{a_G}, \tag{5.2b}$$

$$\Delta J(\psi) = \sum_{r} A^{(r)}(1 - e^{-\psi/\tau_r}) + \sum_{r'} B^{(r')}\psi, \tag{5.2b}$$

*Prepared by W. E. Haisler.

and $A^{(r)}$, $B^{(r')}$ and τ_r are constants. The functions a_G, a_D and $\hat{\sigma}_{cd}$ are material properties and are in general functions of the three stress invariants. The quantity ψ is a reduced time variable while ε_{ab} are engineering strain components and σ_{cd} are components of the Cauchy stress tensor. The function $\Delta J(\psi)$ is the transient component of the so called linear viscoelastic shear creep compliance. The first term in Eq. (5.1) represents the instantaneous elastic response of the material.

To cast Eq. (5.1) into a form suitable for use in an incremental finite element analysis, its time derivative is taken, and Eq. (5.2a) is used to obtain,

$$\dot{\varepsilon}_{ab} = J(o)\dot{\sigma}_{ab} + \frac{\partial(\frac{\partial\hat{\sigma}_{cd}}{\partial\sigma_{ab}})}{\partial t}\int_{-o}^{t}\Delta J(\psi-\psi')\frac{dG_{cd}}{dt'}\,dt'$$

$$+ \frac{a_D}{a_G}\,(\frac{\partial\hat{\sigma}_{cd}}{\partial\sigma_{ab}})\int_{-o}^{t}\frac{d(\Delta J(\psi-\psi'))}{d\psi}\frac{dG_{cd}}{dt'}\,dt' \qquad (5.3)$$

Equation (5.3) is rewritten as

$$\dot{\varepsilon}_{ab} = J(o)\dot{\sigma}_{ab} + \frac{\partial(\frac{\partial\hat{\sigma}_{cd}}{\partial\sigma_{ab}})}{\partial t}X_{cd} + \frac{a_D}{a_G}\,(\frac{\partial\hat{\sigma}_{cd}}{\partial\sigma_{ab}})Y_{cd}\,, \qquad (5.4)$$

where

$$X_{cd} = \int_{-o}^{t}\Delta J(\psi-\psi')\frac{dG_{cd}}{dt'}\,dt'\,, \qquad (5.5)$$

$$Y_{cd} = \int_{-o}^{t}\Delta J'(\psi-\psi')\frac{dG_{cd}}{dt'}\,dt'\,, \qquad (5.6)$$

and

$$\Delta J'(\psi-\psi') = \frac{d\,\Delta J(\psi-\psi')}{d\psi}\,. \qquad (5.7)$$

A time marching procedure for evaluating X_{cd} and Y_{cd} is given in [21].

The evaluation of the two integrals X_{cd} and Y_{cd} given by Eqs. (5.5) and (5.6) represents a key element in evaluating the creep strain rate. Once the values of these integrals are known, the creep strain rate is evaluated from the sum of the second and third terms of Eq. (5.4) as:

$$\dot{\varepsilon}^{c}_{ab} = \frac{\partial(\frac{\partial\hat{\sigma}_{cd}}{\partial\sigma_{ab}})}{\partial t} X_{cd} + \frac{a_D}{a_G}(\frac{\partial\hat{\sigma}_{cd}}{\partial\sigma_{ab}}) Y_{cd} . \tag{5.8}$$

The material parameter a_G, a_D, $\hat{\sigma}_{cd}$, and ΔD are evaluated from standard creep and recovery tests. Details are provided in [20, 22]. In some special cases it is possible to "back-out" these material properties from creep equations as outlined in [21].

In the computer program, these material properties may be input either in functional form or piece-wise linear, tabular form.

In the finite element program, the creep strains predicted by Eq. (5.8) are superimposed with elastic and time-independent plastic strains predicted by an incremental plasticity theory using a kinematic-isotropic hardening model and von Mises yield condition. Limited comparison with experimental data indicates relatively good correlation for non metals and some metals at elevated temperature. Final numerical results are pending on the completion of Sanders work [22].

6. STRUCTURE-PROPERTY STUDIES OF RESIN*

6.1 Differential Scanning Calorimeter (DSC) Investigations

Several other workers have studied physical aging of thermoplastics (in contrast to thermosets, which we have investigated) using the DSC. They find that the shape and position of glass transition changes as the sample is aged. Qualitatively, this is understood by the free volume gradually annealing from the sample. In some cases they found quantitative effects that they could relate to mechanical properties. We endeavored to extend their type of study to a graded series of epoxy resins. However, the attempt to measure aging of a series of epoxy resins by means of changes in the specific heat near the glass transition temperature, T_g, has been abandoned, at least temporarily. The effects we have seen are small and buried in experimental noise so that interpretation has been difficult. This result parallels the small effect of aging observed in another part of this program in the mechanical characteristics of one of the structural epoxy resins, as discussed in the Third Annual Report [1].

The change from thermoplastics to thermosets has two deleterious effects on the study. First, the thermosets we studied have higher glass transition temperatures than the thermoplastics studied in the literature. There is a decrease in the magnitude of the change of specific heat as T_g increases. Secondly, the sharpness of the transition is reduced; this may be a result of either an inhomogeneous sample or be inherent in all thermosets. In the particular series of epoxy resins we used, the curing agent

*Prepared by J. S. Ham

is diaminodiphenyl methane, which is a high melting solid. In order to mix this with the resin, the combination must be heated to a moderately high temperature. While the mixture appears to be well mixed and visibly homogeneous, there can be heterogeneities on a molecular scale that would not be visible to the eye. Theoretically, one would expect the equilibrium condition for an uncured mixture to be homogeneous; but phase separation is quite possible as the cure proceeds since even small positive enthalpies of interaction can become important with curing underway. If this phase separation were to occur late in the crosslinking step, then the fineness of the phases would result in a material that is apparently, but not actually, homogeneous.

There is considerable discussion in the literature concerning the general presence of heterogeneities in both thermosets and thermoplastics. Some electron microscope images show a texture that has been interpreted as a fundamental heterogeneity in a wide variety of material including epoxies. Since optical aberrations in the electron microscope can cause a similar texture and since there are not simple experimental tests that will distinguish whether a texture comes from these aberrations or is physical, the question is still open.

In any case, it appears as though the change in specific heats is small and occurs over a wider temperature range in our samples when compared to the thermoplastics studied in the literature. These factors make the small differences due to aging even harder to distinguish from background noise.

In addition, the epoxy resins are sensitive to traces of moisture and this modifies the DSC trace as much as aging. We endeavored to control the moisture environment of our samples but some anamolous runs are

attributed to a failure to control moisture adequately.

The combination of a small and diffuse effect in the specific heats and the inherent scatter in the DSC measurements have kept us from observing any systematic effects of aging in our samples.

Attempts to improve the precision of the DSC have not been very fruitful. Although there are some reports in the literature as to how this has been done, we have not succeeded in obtaining results which permit the study we set out to do. Further studies of physical aging will be postponed until we acquire testing equipment which is sufficiently sensitive to changes in mechanical or thermal properties.

6.2 Toughened Resins

The summer of 1981 was spent at the Air Force Materials Laboratory (AFML), Wright Aeronautical Laboratories, where a study on toughening mechanisms in high temperature resins was continued. A report on the 1980 summer's work has been written, accepted, and proofed for a technical report, "Toughening of ATX Resins"; it is now in press.

The AFML has a program to develop a generation of high temperature resins. A wide variety of resins is being developed in which rather short chain compounds are crosslinked through terminal acetylene groups. One can utilize a wide variety of backbone chains with the same crosslinking reaction, can achieve high thermal stability, and can start with relatively low molecular weights. Therefore the understanding of the general properties of these compounds should enable selection of a good resin to be used in composites.

These materials can be made in many different compositions, but tend to be quite expensive to prepare in experimental quantities. It is therefore of importance to understand as much about these compounds as possible

before initiating a large scale program. The flexibility in composition should enable choosing a very attractive resin if the various tradeoffs are clearly understood. One of the factors limiting the success of such a resin is the toughness of the resin and of the composite made from it. The relationship of these quantities from fracture behavior to the molecular structure is mostly conjecture at this time. Yet the payoff of any understanding is great. Therefore, the summer of 1981 was spent at AFML primarily seeking molecular parameters likely to be related to toughness in fractionated samples of the corresponding thermoplastic materials.

Fractions were obtained from P-1700 and P-1800 polysulfone thermoplastics, which are similar in backbone structure to the ATS resins, and fractions were obtained from PPQ-401, a polyphenylquinoxaline thermoplastic which is similar to the backbone structure of another family of acetylene terminated compounds considered as a potential high temperature resin.

Dilute solution viscosity was used to establish the random coil configuration of the molecules in solution.

The viscosity of more concentrated solutions showed an interaction at very low apparent entanglement lengths. It was observed that this critical concentration for interaction between chains varied as $M^{-1/2}$ rather than as M^{-1} found for flexible chains. A mathematical model for this interaction has been developed and is in preparation for publication. The feature responsible for this behavior in the critical concentration is, according to this model, the rigidity of the chains. It is not necessary for a rigid chain to have the conformation of a rigid rod, but it can have the conformation of a random walk if the rotational transitions of the bonds is very slow.

High temperature measurements on the undiluted polymers indicate

that at these high temperature, the chains are flexible and entangle as flexible chains.

The relationship of these observations to toughening of the resins and composites has yet to be made; but the conjecture is that the crosslink spacing must be no less than the distance between entanglements in order to obtain the maximum elongation at break. Higher crosslink density would make the material more brittle and produce a higher glass transition temperature. Lower crosslink density would give little benefit.

Several papers on these topics are in various stages of preparation as part of my effort on the AFOSR project.

6.3 Viscoelastic Behavior

A molecular model for creep is in the early stages of development. Rather general and plausible assumptions can lead to a creep function of $A \exp kt^{1/3}$, which matches a variety of experimental studies. Other exponents are possible depending upon the assumptions. It is not clear whether this type of creep behavior is due to statistically homogeneous molecular motion or if it is a property of cracking, crack healing, or other phenomena on a scale large compared to molecular dimensions.

7. GRADUATE RESEARCH ASSISTANT ACTIVITIES

7.1 Summary

The third group of graduate engineering students to participate on the M.S. level in the AFOSR research project entered the program in September 1980. They now have completed all of their requirements for a Master of Science degree, and the results of the research are reported in the following theses:

1. Arenburg, R.T., "Analysis of the Effect of Matrix Degradation on Fatigue Behavior of a Graphite/Epoxy Laminate."

2. Braswell, J.L., "The Effect of Geometry on the Design of Filament-Wound Fiberglass Tension Lugs."

3. Coulter, B.A., "Transverse Shear Deformation Effects in Composite Laminated Plates."

4. Cullen, J.S., "Mode I Delamination of a Unidirectional Graphite/Epoxy Composite Under Complex Load Histories."

5. Earley, J.W., "Compression Induced Delamination in a Unidirectional Graphite/Epoxy Composite."

6. VanderKley, P.S., "Mode I - Mode II Delamination Fracture Toughness of a Unidirectional Graphite/Epoxy Composite."

7. Williams, D.R., "Mode I Transverse Cracking in an Epoxy and a Graphite Fiber Reinforced Epoxy."

The abstracts are collected in subsection 7.2. Copies of the theses will be provided upon written request to the Principal Investigator (R.A. Schapery).

The current group consists of three M.S. and four Ph.D. students. Besides conducting research on this project, the students are involved in academic courses, as noted in the program announcement in Appendix B.

7.2 Abstracts of M.S. Theses

ABSTRACT

Analysis of the Effect of Matrix Degradation on Fatigue Behavior of a Graphite/Epoxy Laminate. (May 1982)

Robert Thomas Arenburg, B.C.E.T., Southern Technical Institute

Chairman of Advisory Committee: Dr. R. A. Schapery

An analytical study of the effect of fatigue on a $[\pm 45/90_2]_s$ graphite/epoxy laminate is conducted considering two levels of damage. The first one is microscopic damage, which is viewed as a matrix softening mechanism that is accounted for by the use of micromechanics. The second level of damage is delamination. An evaluation of lamination theory versus a finite element elasticity solution which accounts for free edge stresses is made first. Lamination theory is found to be inadequate due to its inability to account for large amounts of shear deformation as the matrix degrades. Experimental data are used to evaluate the matrix degradation as a function of fatigue cycles, and then a parametric study of the strain energy release rate as a function of delamination size at various degrees of matrix degradation is conducted. For a constant maximum stress fatigue test, the matrix degradation leads to an increase in strain energy which is predicted to eventually cause rapid delamination. Reasonably good agreement between theory and experimental data on the $[\pm 45/90_2]_s$ laminate is demonstrated.

ABSTRACT

The Effect of Geometry on the Design of Filament-Wound Fiberglass Tension Lugs. (December 1981)

James Lee Braswell, Jr., M.S., Texas A&M University

Chairman of Advisory Committee: Dr. Richard M. Alexander

Finite element analysis is employed to characterize the mechanical behavior of filament-wound fiberglass racetrack style tension lugs as a function of lug geometry. The effect on ultimate load carrying capability and the location of failure origination due to static loads applied uniaxially to S2/E773 glass/epoxy specimens is considered. Three configurations are studied, each having identical cross-sectional areas. They differ only in the path the fibers traverse around the pin. In the baseline case, the path is semi-circular. The other two follow semi-elliptical paths with the major diameter of the ellipse aligned with the direction of the applied load. The major to minor diameter ratios are 1.5 and 2.0. Stress distributions at various locations of interest are calculated and presented graphically. The lug failure load and fracture initiation site is predicted for each configuration. The predictions are based on the maximum stress criterion of failure and published material property data. From these analytical results it is concluded that increased structural efficiency can be obtained by taking advantage of the shape latitude available through filament winding.

Experimental data used to verify the analysis is obtained by loading seven specimens of each lug shape to failure. Two of the seven specimens

are strain gaged in locations compatible with the finite element grid to aid in checking the analytical results. Weibull location parameters are determined for each lug shape and expected failure loads are compared to those predicted by the analysis. Reasonably good predictions are made for two of the three lug shapes regarding failure strength and location of failure initiation. Accurate results for the third require additional considerations not treated here.

ABSTRACT

Tranverse Shear Deformation Effects

In Composite Laminated Plates. (December 1981)

Brett Ainsley Coulter, B.S., Math., Colorado School of Mines

B.S., C.E., University of Colorado

Chairman of Advisory Committee: Dr. Y. Weitsman

This thesis presents a closed-form displacement solution for a composite rectangular plate loaded normal to its surface. A high-order plate theory with eight independent displacement functions is used and the mid-plane deflection solution is compared with the solution obtained from classical plate theory, which admits only three independent functions.

The analysis provides the elastic solution for a laminated plate made of a graphite/epoxy material. Several laminate lay-ups, plate aspect ratios and width-to-thickness ratios are considered. Visco-elastic damping, excluding inertia effects, is also considered with frequency covering a wide spectrum.

ABSTRACT

MODE I Delamination of a

Unidirectional Graphite/Epoxy Composite

Under Complex Load Histories (December 1981)

James Scott Cullen, B.S. Civil Engineering

University of Massachusetts

Chairman of Advisory Committee: Dr. K.L. Jerina

A split laminate beam specimen is used to obtain the relationship between energy release rate and crack speed in a unidirectional graphite/epoxy composite under ambient and elevated temperature and humidity environments for pure Mode I delamination. The analysis employs a linear elastic fracture mechanics approach coupled with non-linear beam theory to account for the large deflections and rotations produced experimentally.

ABSTRACT

Compression Induced Delamination in a

Unidirectional Graphite/Epoxy Composite (Dec. 1981)

John William Earley, B.S. Aeronautical Engineering

California Polytechnic State University

Chairman of Advisory Committee: Dr. K.L. Jerina

The opening mode delamination fracture toughness of a graphite/epoxy composite subjected to axial compression and a constant side load was investigated experimentally. Energy release rate for a stably growing crack (G_{IC}) was determined using linear beam-column theory and linear elastic fracture mechanics analysis.

The experimental program consisted of a symmetric graphite/epoxy beam-column arrangement simultaneously subjected to axial and lateral loads. The results from the study indicated good agreement between theoretical and experimental displacements, and a good prediction of Mode I critical strain energy release rate (G_{IC}). An energy release rate of 137.30 N-m/m^2 (.784 in-lb/in^2) was determined in general for the AS1-3502 graphite/epoxy.

ABSTRACT

Mode I - Mode II Delamination Fracture Toughness of a Unidirectional Graphite/Epoxy Composite. (December 1981)

Peter Stephen VanderKley, B.S., University of Michigan

Chairman of Advisory Committee: Dr. Walter L. Bradley

The delamination fracture toughness of a graphite/epoxy composite under varied mode I (opening)/mode II (in-plane shear) load ratios is investigated experimentally. The critical energy release rate $G_{(I, II)c}$ is determined using a double cantilevered beam specimen, linear elastic fracture mechanics, linear beam theory, and analysis of an asymmetric loading scheme by superposition of solutions for pure opening and pure bending components. $G_{(I, II)c}$ was found to range from 190 to 590 N/m with the higher values observed for greater Mode II contribution. A history effect was also observed with high mode II components early in the test giving higher $G_{(I, II)c}$ values later in the test. Fractographs of fracture surface indicate a correlation between fiber/fiber bundle pullout and $G_{(I, II)c}$. Delamination cracking under mode II loads traversed entire ply thickness resulting in considerable fiber breakage and pullout, which accounts for the dramatic increase in initial energy release rate as compared to pure mode I delamination where G_{Ic} is found to be 140-160 N/m.

ABSTRACT

Mode I Transverse Cracking in an Epoxy and a Graphite Fiber Reinforced Epoxy. (December 1981)
David Robert Williams, B.S., Rice University
Chairman of Advisory Committee: Dr. Walter L. Bradley

Opening mode transverse fracture is studied in an epoxy resign with and without graphite fiber reinforcement. Energy absorption rate and critical stress intensity for fracture are determined using compact tension specimens tested under intermittent fixed grip conditions. The graphite/epoxy composite manifests a significant increase in fracture toughness with crack length as the crack length to specimen width ratio (a/w) exceeds 0.5. This increase in toughness is correlated with an increase in fiber breakage and pullout and permanent matrix deformation. Results obtained in this study are compared with results from studies of delamination fracture toughness of the same composite material to show that transverse fracture toughness is greater than delamination fracture toughness in the graphite/epoxy composite, which is in turn greater than the neat resin toughness for the material studied.

8. PROFESSIONAL PERSONNEL INFORMATION

8.1 Faculty Research Assignments

Each participating faculty member is responsible for the research conducted in at least one specific area of investigation, as shown below. In addition, most serve as chairmen of one or more of the graduate advisory committees for M.S. and Ph.D. students and, as such, direct their students' research project. The faculty also contribute to other research activities on the project by serving on student advisory committees, through technical meetings, informal discussions, and, in some cases, through specific research work.

The Principal Investigator (R. A. Schapery) has responsibility for overall technical direction and coordination and for project management. In addition he has direct responsibility for certain research work, as noted below.

Faculty Member/Departmental Affiliation	Primary Research Responsibility
Dr. Walter Bradley/Mechanical Engineering	Delamination and Fracture Properties.
Dr. Walter Haisler/Aerospace Engineering	Development of Finite Element Models
Dr. Joe Ham/Physics	Resin Toughening and Aging
Dr. Ken Jerina/Civil Engineering (Now at Washington Univ., St. Louis)	Experimental Data Base, Deformation and Failure Property Characterization
Dr. Richard Schapery/Aerospace and Civil Engineering	Principal Investigator and Theoretical Models for Damage Growth and Fracture
Dr. Jack Weitsman/Civil Engineering	Constitutive Relations, Environmental Effects

8.2 Additional Professional Staff

Mechanics and Materials Center

Mr. William Eue - Systems Analyst

Mr. Carl Fredericksen - Electronics Technician

Mr. Bob Harbert - Laboratory Supervisor

8.3 Spoken Papers and Lectures at Conferences and Other Professional Activities of the Faculty Related to Composite Materials (1 January 1981 - 31 December 1981):

W.L. Bradley

Invited Lectures and Conference Presentations:

"Failure Analysis: Methods and Case Histories," Series of lectures given in Mexico, Jan. 1981.

"Fracture: Micromechanisms and Macroscopic Measurements of Toughness" (one day presentation as part of a short course presented at TAMU, Jan. 1981).

"Fracture Toughness Studies of Gray, Malleable and Nodular Iron," AIME Annual Meeting, Chicago, Feb. 1981.

"J-Integral Fracture Toughness Studies in Gray Cast Iron," invited lecture for Metal Properties Council, Feb. 1981.

"Fracture of Commercial Cast Irons," invited lecture to American Foundrymen's Society Annual Meeting, St. Louis, April 1981.

"Fracture Behavior in Cast Irons - An Overview," invited lecture at Lawrence Livermore Laboratories, Aug. 1981.

J.S. Ham

Invited Lectures:

"Designing Resins for Toughness," General Tire, Akron, May 1981 and at Universal Energy Systems, Dayton, Aug. 1981.

"Toughness of ATX Resins," AFML, Dayton, June 1981.

"Entanglements in a Polysulfone," AFML, Dayton, Aug. 1981.

"Physics and Polymer Research," McMurray College, and Abilene Christian University, Abilene, Oct. 1981; American Association of Physics Teachers, Fort Worth, Nov. 1981.

R.A. Schapery

Invited Lectures and Conference Presentations:

"Nonlinear Fracture Analysis of Viscoelastic Composite Materials Based on a Generalized J Integral Theory," Japan-U.S. Conference on Composite Materials, Tokyo, Jan. 1981.

"Dynamic Fracture of Viscoelastic Media," ONR Workshop on Solid Propellant, Washington, D.C., Feb. 1981.

"J Integral Theory for Nonlinear Viscoelastic Media," Univ. of Illinois, Urbana, April 1981.

"Fracture of Composite Materials," Phillips Petroleum, Bartlesville, May 1981.

"Composite Materials for Structural Design," Seventh Annual Mechanics of Composites Review, Dayton, Oct. 1981.

"On Viscoelastic Deformation and Failure Behavior of Composite Materials with Distributed Flaws," ASME Annual Winter Meeting, Washington, D.C., Nov. 1981.

Y. Weitsman

Invited Lectures and Conference Presentations:

"Residual Thermal Stresses in Cross-ply Graphite/Epoxy Laminates," 22nd Joint AIAA/ASME/ASCE/AHS meeting in Atlanta, April 1981.

"Environmental Effects in Polymeric and Composite Materials," Bell Laboratories, Atlanta, April 1981.

"Optimal Cool-Down Paths and Residual Thermal Stresses in Cross-Ply Composite Laminates and Adhesive Joints," 18th Annual Meeting of the Society of Engineering Science, Sept. 1981.

"The Non-Linear Thermo-Viscoelastic Characterization of Adhesives," Univ. of Massachusetts, Amherst, Oct. 1981.

"Stresses in Adhesive Joints due to Moisture Sorption," ASME Annual Winter Meeting, Washington, D.C., Nov. 1981.

"The Thermoviscoelastic Characterization of Polymeric Materials," Bell Laboratories, Atlanta, Nov. 1981.

"Environmental Effects in Composites," the Technion, Haifa, Dec. 1981.

Technical Committee Membership:

AIAA Subcommittee on Design Allowables for Composite Materials.

In addition to the above activities, the faculty attended several conferences on composites, chaired technical sessions, published papers on other projects, and worked as consultants to industry.

9. REFERENCES

1. R.A. Schapery, W.L. Bradley, W.E. Haisler, J.S. Ham, K.L. Jerina, Y. Weitsman, "Composite Materials For Structural Design (Third Annual Technical Report)," Texas A&M University, Report No. MM3724-81-5, February 1981.

2. P.S. VanderKley, "Mode I - Mode II Delamination Fracture Toughness of a Unidirectional Graphite/Epoxy Composite," M.S. Thesis, Texas A&M University, December 1981.

3. R.W. Hertzberg, Deformation and Fracture Mechanics of Engineering Materials, Wiley, New York, 1976, p. 261.

4. J.E. Srawley, "Wide Range Stress Intensity Factor Expressions for ASTM E399 Fracture Toughness Specimens," International Journal of Fracture, Vol. 12 (1976), p. 475.

5. J.F. Mandell, F.J. McGarry, S.S. Wang, and J. Im, "Stress Intensity Factors for Anisotropic Fracture Test Specimens of Several Geometries," J. Composite Materials, Vol. 8, 1974 , p. 106.

6. G.C. Sih and H. Liebowitz, "Mathematical Theories of Brittle Fracture," Fracture, edited by H. Liebowitz, Vol. 2, Academic Press, 1968, p. 67.

7. S.W. Tsai and H.T. Hahn, Introduction to Composite Materials, Technomic, Westport, Connecticut, 1980, pp. 19-20, 388-401.

8. W.D. Bascom, J.L. Bitner, R.J. Moulton, and A.R. Siebert, "The Interlaminar Fracture of Organic Matrix, Woven Reinforcement Composites", Composites, January 1980, p. 9.

9. D.R. Williams, "Mode I Transverse Cracking in an Epoxy and a Graphite Fiber Reinforced Epoxy", M.S. Thesis, Texas A&M University, College Station, TX, 77843, December 1981 .

10. R.C. Hulsey, "Delamination Fracture Toughness of a Unidirectional Graphite/Epoxy Composite," M.S. Thesis, Texas A&M University, December 1980.

11. D.F. Devitt, R.A. Schapery, and W.L. Bradley, "A Method for Determining the Mode I Delamination Fracture Toughness of Elastic and Viscoelastic Composite Materials," Journal of Composite Materials, Vol. 14, 1980, p. 270.

12. M. Ashizawa, "Fast Interlaminar Fracture of a Compressively Loaded Composite Containing a Defect," Presented at Fifth DOD/NASA Conference on Fibrous Composites in Structural Design, January 1981. (Douglas Aircraft Company paper 6994.)

13. S. Yamini and R.J. Young, "Stability of Crack Propagation in Epoxy Resins," Polymer, Vol. 18, 1977, p. 1075.

14. D.C. Phillips, J.M. Scott, M. Jones, "Crack Propagation in an Amine-Cured Epoxide Resin," Journal of Materials Science, Vol. 13, 1978, p. 311.

15. J.M. Scott, G.M. Wells, and D.C. Phillips, "Low Temperature Crack Propagation in an Epoxide Resin," Journal of Materials Science, Vol. 15, 1980, p. 1436.

16. T. Ho and R.A. Schapery, "The Effect of Environment on the Mechanical Behavior of AS/3501-6 Graphite/Epoxy Material, Phase III," Vought Corp., ATC Report No. R-92100/1CR-5, NASC Contract No. N00019-79-C-0580, January 1981.

17. R.A. Schapery, "Correspondence Principles and a Generalized J Integral Theory for Deformation and Fracture Analysis of Nonlinear Viscoelastic Media," Texas A&M University Report Nos. MM 3724-81-1 through -3, 1981.

18. R.A. Schapery, "Nonlinear Fracture Analysis of Viscoelastic Composite Materials Based on a Generalized J Integral Theory," Composite Materials, K. Kawata and T. Akasaka, Eds., Proc. Japan-U.S. Conference, Tokyo, Published by Japan Society for Composite Materials, 1981.

19. R.A. Schapery, "On Viscoelastic Deformation and Failure Behavior of Composite Materials with Distributed Flaws," 1981 Advances in Aerospace Structures and Materials - AD-01, S.S. Wang and W.J. Renton, Eds., Published by ASME, 1981.

20. R.A. Schapery, "Further Development of a Thermodynamic Constitutive Theory: Stress Formulation," Purdue University, Report 69-2, February 1969.

21. D.R. Sanders and W.E. Haisler, "An Incremental Form of the Single Integral Nonlinear Viscoelastic Theory for Elastic-Plastic-Creep Finite Element Analysis," Computers and Structures, 1980.

22. D.R. Sanders, Ph.D. Dissertation, Texas A&M University, in preparation.

APPENDIX A

Recent Publications

1. "A Rapidly Convergent Scheme to Compute Moisture Profiles in Composite Materials Under Fluctuating Ambient Conditions," by Y. Weitsman.

2. "Optimal Cooling of Cross-Ply Composite Laminates and Adhesive Joints," by Y. Weitsman and B.D. Harper.

A Rapidly Convergent Scheme to Compute Moisture Profiles in Composite Materials Under Fluctuating Ambient Conditions

Y. WEITSMAN

Texas A&M University
Professor, Mechanical & Materials Center
Civil Engineering Department
College Station, TX 77843

(Received February 12, 1981)

ABSTRACT

This paper presents a highly efficient numerical scheme to compute the moisture distribution in composite materials and adhesive joints under time varying ambient relative humidities and temperatures. The moisture diffusion is assumed to follow Fick's laws. It is shown that by appropriate switching among the various forms of the analytic solutions, all involving infinite series, it is possible to attain extremely high accuracy by means of a small number of terms.

An example is provided to illustrate the method.

BASIC CONSIDERATIONS

CONSIDER A MOISTURE sorption process that is described by the classical diffusion laws. In the one dimensional case we have

$$\frac{\partial m}{\partial t} = D \frac{\partial^2 m}{\partial x^2} \tag{1}$$

to which we must attach initial and boundary conditions.

In (1) $m = m(x,t)$ is moisture content, x is the spatial coordinate, t is time and D is the coefficient of moisture diffusion.

It has been observed [1,2] that the equilibrium moisture content depends on the ambient relative humdiity, and we shall also assume that the boundary conditions are determined by the same quantity. Furthermore, the moisture diffusivity was found to be most sensitive to tempeature [3,4]. Several empirical relationships were proposed, and we shall employ

Reprinted from Journal of COMPOSITE MATERIALS, Vol. 15 (July 1981)
0021-9983/81/04 0349-10 $04.50/0

$$M = Cr^{\alpha} \tag{2}$$

$$D(T) = D_R \exp\left(A/T_R - A/T\right) \tag{3}$$

In (2) and (3) M is the equilibrium moisture content, r the ambient relative humidity, T the temperature, T_R the reference temperature and A, C, α the material constants.

In accordance with previous analyses [5,6] we can uncouple the process of heat diffusion from all other time-dependent material processes, e.g. moisture-diffusion or stress-relaxation. This simplification is justified because for all practical temperature fluctuations and geometrical dimensions the time required to reach thermal equilibrium is several orders of magnitude shorter than the time-scales for moisture diffusion or for relaxation response. Consequently, we consider spatially uniform temperature profiles, namely $T = T(t)$ as prescribed by the fluctuations in ambient temperature, when analyzing transient moisture diffusion.

SYMMETRIC EXPOSURE

Consider an infinite plate of thickness $2L$. Let $-L \leqslant x \leqslant L$ and assume an initial uniform moisture distribution m_o. When the plate is exposed to an elevated ambient relative humidity the boundary moisture is given by μ, namely $m(x = \pm L, t) = \mu$. Due to the symmetry of the present problem it suffices to analyze only the region $0 \leqslant x \leqslant L$.

For constant μ the moisture content $m(x,t)$ is given by well known expressions [7,8]. Since we aim at extending those expressions to the case of fluctuating $\mu(t)$ and temperature $T(t)$ we choose to represent them in the following form

$$m(x,t) - m_o I_o(x,t) = \mu\, I(x,t) \tag{4}$$

The functions $I_o(x,t)$ and $I(x,t)$ take two alternate forms

$$I_o(x,t) = \begin{cases} C(x,t) \\ \text{or} \\ 1 - E(x,t) \end{cases}, \quad I(x,t) = \begin{cases} 1 - C(x,t) \\ \text{or} \\ E(x,t) \end{cases} \tag{5}$$

In (5)

$$C(x,t) = -2 \sum_{n=1}^{\infty} (-1)^{n+1} \cos(p_n x/L) \exp(-p_n^2 t^*) \tag{6}$$

and

$$E(x,t) = \sum_{n=1}^{\infty} (-1)^{n-1} \left[\operatorname{erfc}\left(\frac{2n-1-x/L}{2\sqrt{t^*}}\right) + \operatorname{erfc}\left(\frac{2n-1+x/L}{2\sqrt{t^*}}\right)\right] \tag{7}$$

$$\text{with } p_n = (2n-1)\pi/2 \quad \text{and } t^* = Dt/L^2 \tag{8}$$

The complementary error function erfc(z) decays rapidly with z. Its asymptotic value is given by [9] erfc $z \sim (\sqrt{\pi}z)^{-1} \exp(-z^2)$ consequently, for computational precision of $0(10^{-16})$ — as obtains in "double precision" routines in digital computers — we can set erfc $z = 0$ for $z > 5.877$. In the sequel we shall designate this "cut-off" number by λ.

The rapid decay of erfc z implies that series (7) converges rapidly for short times. On the other hand it is obvious that series (6) converges rapidly for long times. To achieve computational efficiency we should therefore switch among the two forms of equations (5).

Straightforward arithmetic yields that accuracy of $0(10^{-16})$ is maintained by the following set of rules

$$\text{for} \quad \left(\frac{i-1}{2\lambda}\right)^2 < t^* < \left(\frac{i}{2\lambda}\right)^2 \quad \text{use } i \text{ terms in series (7)} \tag{9a}$$

$$\text{for} \quad \left(\frac{5}{2\lambda}\right)^2 < t^* < \left(\frac{Q}{9^2}\right) \quad \text{use five terms in series (6)} \tag{9b}$$

$$\text{for} \quad \frac{Q}{(2i+1)^2} < t < \frac{Q}{(2i-1)^2} \quad \text{use } i \text{ terms in series (6)} \tag{9c}$$

In (9a) and (9c) i = 1, 2, 3, 4. Also $Q = 14.93$ and $\lambda = 5.877$.

For $t^* > Q$ the moisture distribution is uniform to within $0(10^{-16})$.

It follows from (9a) that we never need more than the four following terms in series (7):

$$\text{erfc}\left(\frac{1-x/L}{2\sqrt{t^*}}\right) + \text{erfc}\left(\frac{1+x/L}{2\sqrt{t^*}}\right) - \text{erfc}\left(\frac{3-x/L}{2\sqrt{t^*}}\right) - \text{erfc}\left(\frac{3+x/L}{2\sqrt{t^*}}\right)$$

It can be noted that the form of expressions (9) remains valid for *any* desired accuracy ε, except that λ and Q depend on ε. Obviously for a lesser accuracy we require even fewer terms in (6) and (7).

Consider now the case of fluctuating temperatures, $T = T(t)$. In view of (3) the diffusivity D is now time dependent and the non-dimensional time t^* in (8) becomes a complicated function of real-time t. However, if we consider $t^* = D_R t/L^2$ at the reference temperature $T = T_R$ then in analogy with thermoviscoelasticity [10] we can replace t^* with the reduced dimensionless time ξ^* whenever $T = T(t)$ as follows

$$\xi^* = \frac{D_R}{L^2} \int_0^t \exp[A/T_R - A/T(s)]ds \tag{10}$$

The moisture distribution under fluctuating temperatures is given by (4) with t^* replaced by ξ^*. In view of the single-valuedness of $\xi^* = \xi^*(t)$ it is always possible to convert the results back to real time t.

Consider next the case of fluctuating ambient relative humidity $r = r(t)$. By equation (2) this implies $\mu = \mu(t)$. When $\mu = \mu(t)$ and $T = T(t)$ equation (4) yields, upon employment of the superposition integral

$$m(x,t) - m_o I_o(x,\xi^*) = \int_0^t I[x,\xi^*(t) - \xi^*(\tau)]\,\mu'(\tau)d\tau \tag{11}$$

Equation (11) must of course be evaluated numerically.

NON-SYMMETRIC EXPOSURE

Consider now an infinite plate of thickness L whose faces $x = 0$ and $x = L$ are exposed to different relative humidities which fluctuate independently of each other. We still assume that all temperature fluctuations are spatially uniform within the entire plate.

The solution to differing, but constant boundary conditions $m(o,t) = \mu^\circ$ and $m(L,t) = \mu^L$ with zero initial moisture $m(x,o) = o$ can be expressed as follows

$$m(x,t) = \mu^{\circ} H_o(x,t^*) + \mu^{l} H_L(x,t^*) \tag{12}$$

with

$$H_o(x,t^*) = \begin{cases} S_o(x,t^*) \\ \text{or} \\ U_o(x,t^*) \end{cases} \qquad H_L(x,t^*) = \begin{cases} S_L(x,t^*) \\ \text{or} \\ U_L(x,t^*) \end{cases} \tag{13}$$

In (13)

$$S_o(x,t^*) = 1 - \frac{x}{L} - \frac{2}{\pi} \sum_{n=1}^{\infty} \frac{1}{n} \sin \frac{q_n x}{L} \exp(-n^2\pi^2 t^*) \tag{14}$$

$$S_L(x,t^*) = \frac{x}{L} + \frac{2}{\pi} \sum_{n=1}^{\infty} \frac{\cos n\pi}{n} \sin \frac{q_n x}{L} \exp(-n^2\pi^2 t^*)$$

$$U_o(x,t^*) = \operatorname{erfc}\left(\frac{x/L}{2\sqrt{t^*}}\right) + V_o(x,t^*) - W_o(x,t^*) \tag{15}$$

$$U_L(x,t^*) = \operatorname{erfc}\left(\frac{1 - x/L}{2\sqrt{t^*}}\right) + V_L(x,t^*) - W_L(x,t^*)$$

The functions V and W in (15) represent the following infinite series

$$V_o(x,t^*) = \sum_{n=1}^{\infty} \operatorname{erfc}\left(\frac{2n + x/L}{2\sqrt{t^*}}\right)$$

$$W_o(x,t^*) = \sum_{n=0}^{\infty} \operatorname{erfc}\left(\frac{2(n+1) - x/L}{2\sqrt{t^*}}\right) \tag{16}$$

(Continued)

$$V_L(x,t^*) = \sum_{n=1}^{\infty} \operatorname{erfc}\left(\frac{2n + 1 - x/L}{2\sqrt{t^*}}\right) \tag{16}$$

$$W_L(x,t^*) = \sum_{n=0}^{\infty} \operatorname{erfc}\left(\frac{2n + 1 + x/L}{2\sqrt{t^*}}\right)$$

In (12—16) $t^* = Dt/L^2$ and $q_n = n\pi$.

Expressions (14) are available in the literature [8], while (15) are obtained by means of a straightforward Laplace transform and inversion method.

Maximal efficiency in evaluating H_o and H_L is again obtained by switching between their alternate forms given in (13) and detailed in (14—16), because (14) is efficient for long times and (15) is advantageous for short times. For instance, for an accuracy of $0(10^{-16})$ we never need more than four terms in each of U_o, U_L, S_o and S_L as listed in Table 1 below. For a lesser accuracy the number of terms is of course smaller.

Table 1. Number of Terms Required in Various Truncated Series to Attain Accuracy of $0(10^{-16})$ in Moisture Profile ($\lambda = 5{,}877$, $R = 16/\pi^2 \log e$)

Range	Largest Number of Terms in Each Series						Total Number Terms in (12)
	V_o	V_L	W_o	W_L	S_o	S_L	
$0<t^*<(\frac{1}{\lambda})^2$	0	0	0	0	0	0	2
$(\frac{1}{\lambda})^2<t^*<(\frac{3}{2\lambda})^2$	1	1	0	0	0	0	4
$(\frac{3}{2\lambda})^2<t^*<(\frac{2}{\lambda})^2$	1	1	1	1	0	0	6
$(\frac{2}{\lambda})^2<t^*<\frac{R}{5}$	2	2	1	1	0	0	8
$\frac{R}{(i+1)}<t^*<\frac{R}{i}$ $(i=4,3,2,1,0)$	0	0	0	0	i	i	2i

For fluctuating boundary conditions $\mu^o(t)$ and $\mu^L(t)$, and with varying temperature $T(t)$ we employ the reduced time ξ^* given in (10) and a superposition integral analogous to (11) to get

$$m(x,t) = \int_0^t \left\{ H_o\,[x,\ \xi^*(t) - \xi^*(\tau)]\ \frac{d\mu^\circ(\tau)}{d\tau} \right. \tag{17}$$

$$\left. + H_L\ [x, \xi^*(t) - \xi^*(\tau)]\ \frac{d\mu^L(\tau)}{d\tau} \right\} d\tau$$

THE NUMERICAL SCHEME

To compute the moisture $m(x,t)$ we divide the time-span of interest t_f into n, not necessarily equal, sub-intervals. These intervals $\Delta_i = t_i - t_{i-1} (i = 1, 2, \ldots n)$ with $t_o = 0$ and $t_n = t_f$ should be selected in a manner that *both* the ambient moistures $\mu^\circ(t)$ and $\mu^L(t)$ as well as the temperature $T(t)$ are represented to within a satisfactory approximation by the "staircase" functions[1]

$$\mu^\circ(t) = \mu_i^\circ, \qquad \mu^L(t) = \mu_i^L. \qquad T(t) = T_i$$

for (18)

$$t_{i-1} < t < t_i \quad (i = 1, 2, \ldots n)$$

Note that in the symmetric case $\mu_o = m_o$.

Denote $g_i = \exp(A/T_R - A/T_i)$ then (10) yields

$$\xi_i^* = \frac{D_R}{L^2} \sum_{k=1}^{i} (t_k - t_{k-1})\, g_K \quad (i = 1,2, \ldots n) \tag{19}$$

Thereby

$$\xi_{ij}^* = \xi_i^* - \xi_j^* = \frac{D_R}{L^2} \sum_{k=j+1}^{i} (t_k - t_{k-1})\, g_k \tag{20}$$

$$(j = 0, 1, \ldots i - 1,\ i = 1, 2, \ldots n)$$

[1]Obviously, only one ambient moisture $\mu(t)$ is involved in the symmetric case.

The integrals (11) and (17) are now represented respectively by the sums

$$m(x,t_i) = m_o I_o(x,\xi_i^*) + \sum_{j=1}^{i} (\mu_o - \mu_{j-1})\, I(x,\zeta_{ij}^*) \tag{21}$$

and

$$m(x,t_i) = \sum_{j=1}^{i} [(\mu_j^\circ - \mu_{j-1}^\circ)\, H_o(x,\zeta_{ij}^*) + (\mu_j^L - \mu_{j-1}^L)\, H_L(x,\zeta_{ij}^*)] \tag{22}$$

Expressions (21) and (22) remain valid for any intermediate time $\hat{t}_i$ *where* $t_{i-1} < \hat{t}_i < t_i$, provided we substitute the value of $\hat{t}_i$ in place of t_i in (19) and (20) as well as in (21) and (22).

Computational efficiency is achieved by switching between the two alternate forms given in (5) and (13) which is accomplished by testing the ranges of ξ_i^* and ζ_{ij}^* according to rules (9a—9c) or in Table 1, respectively. Obviously ξ_i^* and ζ_{ij}^* must replace t^* in equations (9) and in Table 1.

2A NUMERICAL EXAMPLE FOR THE SYMMETRIC CASE

To illustrate the method we consider the case of a sixteen ply 5208/T300 graphite/epoxy laminate with $L = 0.04''$. For this material $D_R = 1.5019 \times 10^{-6}$ in²/min and $A = 6340$.

The composite laminate was considered to be exposed to fluctuating ambient relative humidity, which is reflected as a fluctuating boundary moisture μ, and to fluctuating temperatures.

Specifically, we considered the situation in which the ambient moisture level switched between ½% and 1% every 5000 minutes, while the temperature varied between two fixed levels of 350°K and 297°K also every 5000 minutes. Computations were performed for moisture and temperature fluctuating in phase (case 1) and out of phase (case 2). Case 1 is shown by solid lines and case 2 is marked by dashed lines in Figure 1.

The results, exhibited in Figure 1, show the variation of moisture level with time at a station located at $x = 0.035''$.

Note that sharp slopes in $m(x, t)$ vs. t occur during the high-temperature time intervals. Consequently the in-phase case approaches the saturation level of $m(x, t) = 1\%$ during the "wet" intervals while for the out-of-phase case the moisture level at $x = 0.035''$ approaches 0.5% during the "dry" intervals. The details are shown by the heavy lines in Figure 1.

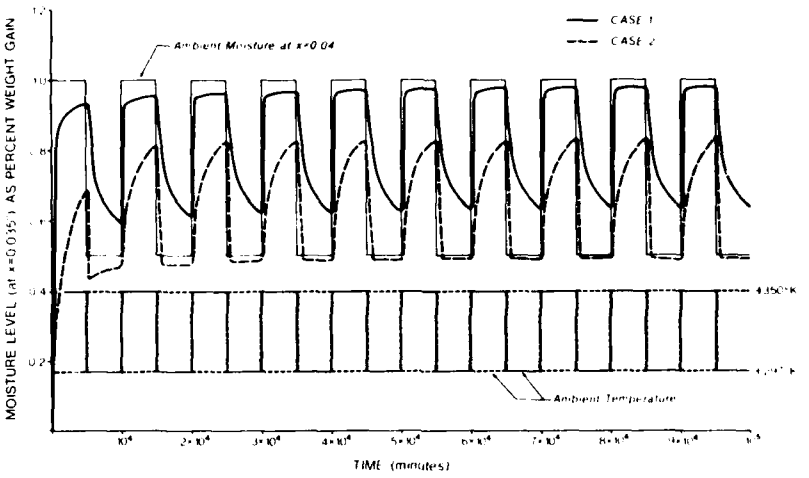

***Figure 1.** Moisture levels at x = 0.035" vs. time in a 0.08" thick 5208/T300 graphite/epoxy laminate that is exposed symmetrically to two cases of fluctuating ambient relative-humidity and temperature. Case 1: R.H. In-phase with temperature. Case 2: R.H. Out-of-phase with temperature.*

ACKNOWLEDGMENTS

This work was conducted, in part, under Contract F33615-79-C-5517 from the Air Force Material Laboratory (AFML/AFWAL) and in part under Contract F 49620-78-C-003 from the Air Force Office of Scientific Research (AFOSR). This support is gratefully acknowledged.

REFERENCES

1. Shen, C. H. and Springer, G. S., "Moisture Adsorption and Desorption of Composite Materials," *Journal Comp. Mat.*, Vol. 10, Jan. 1976, pp. 36—54.
2. Delasi, R. and Whiteside, J. B., "Effect of Moisture on Epoxy Resins and Composites." In Advanced Composite Materials — Environmental Effects, STP 658 (ASTM), J. R. Vinson — Editor, 1978, pp. 2—20.
3. Shirrel, C. D., "Diffusion of Water Vapor in Graphite/Epoxy Laminates." In Advanced Composite Materials — Environmental Effects, STP 658 (ASTM) J. R. Vinson — Editor, 1978, pp. 21—42.
4. McKague, E. L. and Halkias, J. E., Private Communication.
5. Weitsman, Y., "Diffusion With Time-Varying Diffusivity, With Application to Moisture-Sorption in Composites," *Journal Compt. Mat.*, Vol. 10, July 1976, pp. 193—204.
6. Douglass, D. A. and Weitsman, Y., "Stresses Due to Environmental Conditioning of Cross-Ply Graphite/Epoxy Laminates," Proc. Third International Conference on Composite Materials (ICCM3), Paris, France. A. R. Bunsell et. al., Editors, Vol. 1, pp. 529—542, Pergamon Press (1980).

7. Luikov, A. V., "Analytical Heat Diffusion Theory," Academic Press, 1968, pp. 97—114.
8. Crank, J., "The Mathematical Theory of Diffusion," Oxford University Press, 2nd ed., 1975, pp. 47, 104—105.
9. Abramowitz, M. and Stegun, L. A., "Handbook of Mathematical Functions," National Bureau of Standards, June 1964, p. 298.
10. Morland, L. W. and Lee, E. H., "Stress Analysis for Linear Viscoelastic Materials With Temperature Variation," *Transactions Society of Rheology,* Vol. IV, 1960, pp. 233—263.

MM 3724-81-7
April 1981

Optimal Cooling of Cross-Ply Composite Laminates and Adhesive Joints

by

Y. Weitsman* and B. D. Harper**

Abstract

This paper concerns the optimal cooling of symmetric, balanced, cross-ply composite laminates and of adhesive joints so as to minimize the residual thermal stresses upon termination of the cool-down process.

The computations are based upon a recently developed analytical scheme and employ up-to-date data on graphite/epoxy laminae. The calculations consider the thermoviscoelastic response of the polymeric resins and incorporate the temperature dependence of the coefficients of thermal expansion.

It is shown that the viscoelastic behavior may contribute to a significant reduction of the residual stresses.

---

*Professor, Mechanics and Materials Center
**Graduate Student
Texas A&M University
College Station, Texas 77843

Introduction

This paper presents results based upon a recently developed optimization scheme[1]*§ and data on viscoelastic response of graphite/epoxy composites[3] whereby specific time-temperature paths are selected during the cool-down stage so as to minimize the residual thermal stresses in cross-ply laminates and in adhesively bonded alumimum/epoxy joints.

The cross-ply laminates under consideration consist of a symmetric and balanced lay-up of 0° and 90° plies. When such laminates are cooled from the presumed stress-free cure temperature down to room temperature the stiffer fibers within each ply restrain the transverse shrinkage of the adjacent, perpendicularly directed, plies and these mutual geometric constraints introduce substantial residual stresses in the laminate.

Since temperature causes thermal expansion against geometric constraints it can be viewed as a stress inducing agent. On the other hand, temperature enhances and accelerates the process of stress relaxation. The optimal time-temperature path achieves the best interplay between the above mentioned competing effects so as to minimize the residual thermal stress at the termination of the cool-down phase.

Elastic Analysis

Consider a symmetric, balanced, cross-ply composite laminate, consisting of equal number of 0° and 90° plies exposed to fluctuating ambient temperature T(t). In view of the small thicknesses of the composite laminates exployed in practice it is permissible to ignore the process of thermal diffusion and employ the approximation that T=T(t) throughout the laminate

*Numbers in brackets indicate reference listed at the end of this paper.
§See also ref. [2] for treatment of the same problem.

A similar circumstance holds also for adhesive joints.

Denoting by subscripts L and T the longitudinal (parallel to fibers) and transverse (perpendicular to fibers) directions, respectively, we have the following stress-strain relations in each individual lamina[4],[5]

$$\begin{aligned} \varepsilon_L - \alpha_L \Delta T &= \frac{\sigma_L}{E_L} - \frac{\nu_{TL}}{E_T}\ \sigma_T \\ \varepsilon_T - \alpha_T \Delta T &= -\frac{\nu_{LT}}{E_T}\sigma_L + \frac{\sigma_T}{E_T} \end{aligned} \tag{1}$$

In (1) ε and σ designate strain and stress, while α, E and ν denote coefficient of thermal expansion, modulus and Poisson's ratio, respectively. ΔT represents temperature difference.

In view of the particular lay-up under consideration we have

$$\sigma_T = -\sigma_L = \sigma, \quad \varepsilon_T = -\varepsilon_L = \varepsilon$$

and straight forward manipulations yield

$$\sigma = -\frac{E_T(\alpha_T - \alpha_L)\Delta T}{(1+\nu_{TL})\left(1+\frac{1+\nu_{LT}}{1+\nu_{TL}}\frac{E_T}{E_L}\right)} \tag{2}$$

For typical graphite/epoxy laminae we have $E_L \sim 20E_T$ (whereby $\nu_{LT} \sim 20\nu_{TL}$). With $\nu_{LT} \simeq 0.28$ we obtain

$$\sigma = -rE_T(\alpha_T - \alpha_L)\Delta T \tag{3}$$

Typically $r \approx 0.90$—0.93.

Alternately, consider two adherend plates - each of thickness h - bonded together by an adhesive layer of thickness a. Let the joint undergo a spatially uniform temperature excursion ΔT.

Elementary calculations then yield

$$\sigma_e = \frac{E_e}{1-\nu_e} \frac{(\alpha_e - \alpha_A)\Delta T}{1 - \frac{1-\nu_A}{1-\nu_e} \frac{E_e}{E_A} \frac{a}{2h}} \tag{4}$$

In (4) subscripts "A" and "e" refer to the adherend and adhesive, respectively. For typical joints $E_A/E_e = 50$ and $h/a = 100$. Consequently (4) simplifies to

$$\sigma_e \cong \frac{E_e}{1-\nu_e} (\alpha_e - \alpha_A)\Delta T \tag{5}$$

Viscoelastic Formulation

Data on graphite/epoxy laminas[3] and on "neat" epoxy resins[6] indicate that E_T and E_e are time and temperature dependent.* The time-dependence can be approximated by the form

$$E = E_o(t+t_o)^{-q} \tag{6}$$

while the temperature-dependence can be related by means of a shift-factor function $a(T)$, with $a(T_R) = 1$, where customarily T_R is room temperature (293°K). Consequently (6) is extended to read

$$E = E_o \left\{ t_o + \left[t/a(T) \right] \right\}^{-q} \tag{7}$$

Available data[3],[6] indicate that $a(T)$ can be expressed by

$$a(T) = \exp\left(-\frac{T}{A} + B\right) \tag{8}$$

Employing the superposition integral, eqns. (3) and (5) yield[7]

*These data are corroborated by many other sources and publications which are not listed here.

$$\sigma(t) = \alpha E_o \int_0^t \left[\int_\tau^t \frac{ds}{a(T(s))} + t_o \right]^{-q} \frac{d\Delta T(\tau)}{d\tau} \, d\tau \qquad (9)$$

In (9) and the sequel, α represents $(\alpha_T - \alpha_L)$ or $(\alpha_e - \alpha_A)$ and E_o absorbs the factors r or $1/(1-\nu_e)$, respectively. It may be noted that although, in a strict sense, $r = r(t)$ the effect of considering constant r involves errors of no more than 1/2% in all practical cases.

Data on graphite/epoxy [3] indicate that α_T and α_L vary significantly with temperature. This aspect of the material response will be considered later.

Optimal Cooling Paths

Consider now the case of cooling from the initial cure temperature T_I down to room temperature T_R in a given time interval t_f. It has been shown [1] that a minimal value of $\sigma(t)$ in (9) is obtained by following an optimal path $T(t)$ which includes an abrupt initial drop from T_I to T_0. This initial drop was given by solving the transcendental equation[1]

$$T_0 - T_I = \frac{a(T_0)}{a'(T_0)} \qquad (10)$$

In the open interval $0 < t < t_f$ the optimal path $T(t)$ was shown to be smooth and continuous, where it is governed by the nonlinear integro-differential equation

$$\frac{dT}{dt} = - \frac{E''(t,t_f)}{E'(t,t_f)} \frac{a'(T(t))}{a(T(t))a''(T(t))} \qquad (11)$$

In (10) and (11) primes indicate derivatives with respect to the argument. Also

$$E(t_1, t_2) = E\left[\int_{t_1}^{t_2} \frac{ds}{a(T(s))} \right]$$

With given E(t), a(T) and T_I, the value of T_0 is determined by (10) and the optimal temperature path can be constructed by iteration through the employment of (11). In most cases the final prescribed temperature T_R is reached through a second abrupt step at time t_f.

A particular simplification occurs for a "power law" response, as expressed in (6) and, in addition, when the shift-factor function is given by (8).

In this case it was shown [1] that the optimal path is given by

$$T = \frac{1}{C} \ln \frac{L}{K + Ct} \tag{12}$$

where, in (12)

$$C = \frac{q}{(q + 1)A} \quad \text{and} \quad L = K \exp(CT_0)$$

The term K is determined as the root of the transcendental equation

$$Ke^{CT_0} = \left[\frac{e^{B} t_0 (K + Ct_f)^{\frac{1}{q}}}{(q + 1)A} \right]^{\frac{q}{q + 1}} \tag{13}$$

Under the simplifications which occur in the present circumstances the iterative process alluded to in [1] reduces to the search for the root K of eqn. (13).

In view of (8) eqn. (10) yields

$$T_0 = T_I - A \tag{14}$$

With the optimal temperature-path prescribed by (12) the stresses

are obtained by direct substitution of (12) into (9). After several manipulations we get

$$\sigma(t) = \alpha E_o \left\{ \int_0^t Q(\tau,t)d\tau + K(T_I - T_o)\, Q(0,t) \right\} \tag{15}$$

where

$$Q(\tau,t) = \frac{t_o^{-q} \left\{ \left(\frac{K+Ct_f}{K+C\tau} \right)^{\frac{1}{q}} \left[\left(\frac{K+Ct}{K+C\tau} \right)^{\frac{1}{q}} - 1 \right] + 1 \right\}}{K+C\tau}$$

$\sigma(t_f^-)$ is obtained by setting $t = t_f^-$ in (15). At $t = t_f^+$ we get

$$\sigma(t_f^+) = \sigma(t_f^-) + \alpha E_o t_o^{-q} (T_f - T_R) \tag{16}$$

Temperature-Dependent Coefficients of Thermal Expansion

Recent data on graphite/epoxy composites indicate that the quantity $(\alpha_T - \alpha_L)$ increases monotonically with temperature. Consequently (9) must be modified to read

$$\sigma(t) = E_o \int_0^t \left[\int_0^t \frac{ds}{a(T(s))} + t_o \right]^{-q} \frac{d}{d\tau} \left[\alpha(T(\tau))\Delta T(\tau) \right] d\tau \tag{17}$$

In (17) $\alpha(T(t)) = \alpha_T(T(t)) - \alpha_L(T(t))$

Consider the thermal strain

$$\varepsilon_{th}(t) = \alpha(T(t))\ \ \Delta T(t) \tag{18}$$

In view of the one-to-one correspondence between ε_{th} and T we have

$$a(T(t)) = \beta(\varepsilon_{th}(t)) \tag{19}$$

Therefore (17) can be re-written as follows:

$$\sigma(t) = E_o \int_0^t \left[\int_\tau^t \frac{ds}{\beta(\varepsilon_{th}(s))} + t_o \right]^{-q} \frac{d}{d\tau} (\varepsilon_{th}(\tau)) \, d\tau \tag{20}$$

Note that (20) is analogous to (9). Accordingly, (10) and (11) yield the following expressions for the optimal path

$$\varepsilon_{th}^{o} - \varepsilon_{th}^{I} = \frac{\beta(\varepsilon_{th}^{o})}{\beta'(\varepsilon_{th}^{o})} \tag{21}$$

and

$$\frac{d\varepsilon_{th}(t)}{dt} = - \frac{E''(t,t_f)}{E'(t,t_f)} \frac{\beta'(\varepsilon_{th}(t))}{\beta(\varepsilon_{th}(t)) \, \beta''(\varepsilon_{th}(t))} \tag{22}$$

In (22) $E(t_1,t_2) = E \left[\int_{t_1}^{t_2} \frac{ds}{\beta(\varepsilon_{th}(s))} \right]$.

Eqns. (21) and (22) can be expressed in terms of a(T) and T through the reintroduction of (18) and (19). We obtain

$$T_o - T_I = \frac{\alpha(T_o)a(T_0)}{\alpha(T_o)a'(T_o) - \alpha'(T_o)a(T_0)} \tag{23}$$

$$\frac{dT}{dt} = - \frac{E''(t,t_f)}{E'(t,t_f)} \frac{a'}{a\left[a'' - a' \frac{2\alpha' + \alpha''(T-T_I)}{\alpha'(T-T_I)}\right]} \tag{24}$$

In (24) $a = a(T(t))$ and $\alpha = \alpha(T(t))$.

The solution for the optimal path $T(t)$ can be generated by means of an iterative scheme, as noted in ref. [1]. However for the AS/3502 and T300/5208 graphite/epoxy systems the data listed in Tables 1 and 2 below indicate that (23) and (24) differ by at most 2% from expressions (10) and (11) which assume constant α. Consequently, we shall retain (12) as our solution for the optimal path even for the variable α case at hand.

We note however, that although the optimal temperature paths remain unaffected by the variation of α, the thermal stresses do differ significantly.

In the particular circumstance that

$$\alpha(T) = \alpha_0 + \alpha_1 T \tag{25}$$

we obtain

$$\sigma(t) = E_0 \left\{ \int Q(\tau,t) \left[\alpha_0 + \alpha_1 (2T(\tau) - T_I)\right] d\tau + K\,\alpha(T_0)(T_I - T_0)\; Q(0,t) \right\} \tag{26}$$

with the same $Q(\tau,t)$ as in (14).

The stress immediately following the initial discontinuity is

$$\sigma(o^+) = E_o t_o^{-q} \alpha(T_o)(T_I - T_o) \tag{27}$$

After the final discontinuity we have

$$\sigma(t_f^+) = \sigma(t_f^-) + E_o t_o^{-q} \left[\alpha(T_f)(T_f - T_I) - \alpha(T_R)(T_R - T_I)\right] \tag{28}$$

Computations

Calculations were performed for two graphite/epoxy materials and for an epoxy/aluminum joint. The data [3],[6] was reduced to conform with expressions (3), (7), (8), and (25) as shown in Tables 1 and 2 below:

Material System		E_o (KN/m^2)	r	q	t_o (min.)	α (cm/cm°K)	A (°K)	B
Graphite/Epoxy	AS/3502	$10^{7.055}$	.9	.00775	1	$\alpha_L = -.217\times10^{-6}$ $\alpha_T = 24.73\times10^{-6}$ (at T = 372°K)	6.258	46.81
	T300/5208	$10^{7.014}$	.93	.00717	1	$\alpha_L = -.593\times10^{-6}$ $\alpha_T = 25.65\times10^{-6}$ (at T 372°K)	6.792	43.14
Aluminum/ Epoxy		$10^{6.54}$	1	.036	.5	$\alpha_e = 5\times10^{-5}$ $\alpha_A = 2.4\times10^{-5}$	7.91	37.05

Table 1: Material Parameters

Material System	α_L (cm/cm/°K)		α_T (cm/cm/°K)	
	α_o (cm/cm/°K)	α_1 (cm/cm/°K^2)	α_o (cm/cm/°K)	α_1 (cm/cm/°K^2)
AS/3502	$-.484\times10^{-6}$	$.72\times10^{-9}$	9.5×10^{-6}	$.41\times10^{-7}$
T300/5208	$-.418\times10^{-6}$	$-.47\times10^{-9}$	11.9×10^{-6}	$.37\times10^{-7}$

Table 2: The Temperature Dependence of the Thermal Expansion Coefficients. $\alpha(T) = \alpha_o + \alpha_1 T$.

In our computations we employed $T_I = 450°K$, $T_R = 293°K$ and considered cooling times t_f = 10, 50, 100, 500, and 1000 minutes.

The integrations (14) and (26) were performed numerically. For this purpose the time interval t_f was divided into n equal sub-intervals $\Delta t = t_f/n$, resulting in intermediate times $t_i = i\,\Delta t$ and intermediate temperatures T_i evaluated by means of (12). It was found that sufficient accuracy was obtained with n=100.

In order to assess the significance of the variation of α with T, we computed (15) with $\alpha = \dfrac{\alpha(T_I) + \alpha(T_R)}{2}$.

The results are shown in Figs. 1-9. In all those figures temperature T is in °K, stress is in MPa and time is in minutes.

Figs. 1 and 2 exhibit the optimal cooling paths T(t), with the accompanying residual stress, generated during the cool-down process of typical aluminum/epoxy joints for cooling times t_f = 50 and 100 minutes, respectively. Note the jump discontinuities at t=o and $t=t_f$.

Analogous results are shown in Fig. 3 and 4 for the 0°/90° T300/5208 laminate and in Figs. 5 and 6 for the 0°/90° AS/3502 laminate.

In all the above figures the optimal temperature paths were determined by (12). We note that those paths "undershoot" the level of room-temperature (293°K), requiring an upward jump at $t = t_f$.

The stresses in Figs. 1 and 2 were computed according to (15) and (16) employing constant α. On the other hand the curves $\sigma(t)$ in Figs. 3-6 were obtained by employing (26)-(28) considering variable α in accordance with Table 2.

The variation of the residual thermal stress $\sigma(t_f^+)$ with the cooling time t_f is shown in Figs. 7-9. Also shown are the variations of the terminal temperature $T_f = T(t_f^-)$ with t_f. Note that a logarithmic scale is employed for t_f.

For comparison purposes we also exhibit by dashed-dotted lines in Figs. 8 and 9 the final residual stresses $\sigma(t_f^+)$ which result from considering a constant, average value of $\alpha_{av} = \frac{\alpha(T_I) + \alpha(T_R)}{2}$ instead of the actual temperature dependent $\alpha(T)$. Shown in dashed lines is the elastic value of $\sigma(t_f^+)$, which is computed with $\alpha = \alpha_{av}$.

We observe that by taking appropriate account of viscoelastic effects it is possible to attain reductions of about 25% in the residual stresses relative to the linear elastic predictions.

Remarks on Data Reduction

The "power law" representation of relaxation or creep data for polymeric resins or fiber-reinforced composites[3] in the form $E(t) = Et^{-q}$, can be surmised from the fact that the plots of log E vs log t are represented by straight lines [3],[6]. The slopes of those lines determine the power q. Obviously, these plots cannot be extrapolated to time $t = 0$, lest $E(0) \to \infty$. Furthermore, creep or relaxation data are unreliable at very short times

because of the dynamic effects that are technically unavoidable at the early stages of experiments.

Finally, it may also be noted that for $E(t) = Et^{-q}$ the optimization scheme (11) fails because it yields $\lim_{t \to o} T'(t) \longrightarrow -\infty$.

To overcome the above mentioned artifact select a certain short time $t = t_s$, at which the data plots are smooth and beyond which $E(t) = Et^{-q}$. The data can then be extrapolated back to $t = o$ employing Taylor's expansion and the result fitted into the form $E(t) = E_o(t+t_o)^{-q}$ of eqn. (6).

It turns out that by letting $E_o = E(1+q)$ and $t_o = t_s$ we obtain representations in the form of (6) that match all data points indistinguishably from $E(t) = Et^{-q}$.

Acknowledgement

The authors wish to thank Mr. W. Eue of Texas A&M University for his help in obtaining the numerical results presented herein.

This work was conducted under Contract F49620-78-C-0034 from the Air Force Office of Scientific Research (AFOSR) whose support is gratefully acknowledged.

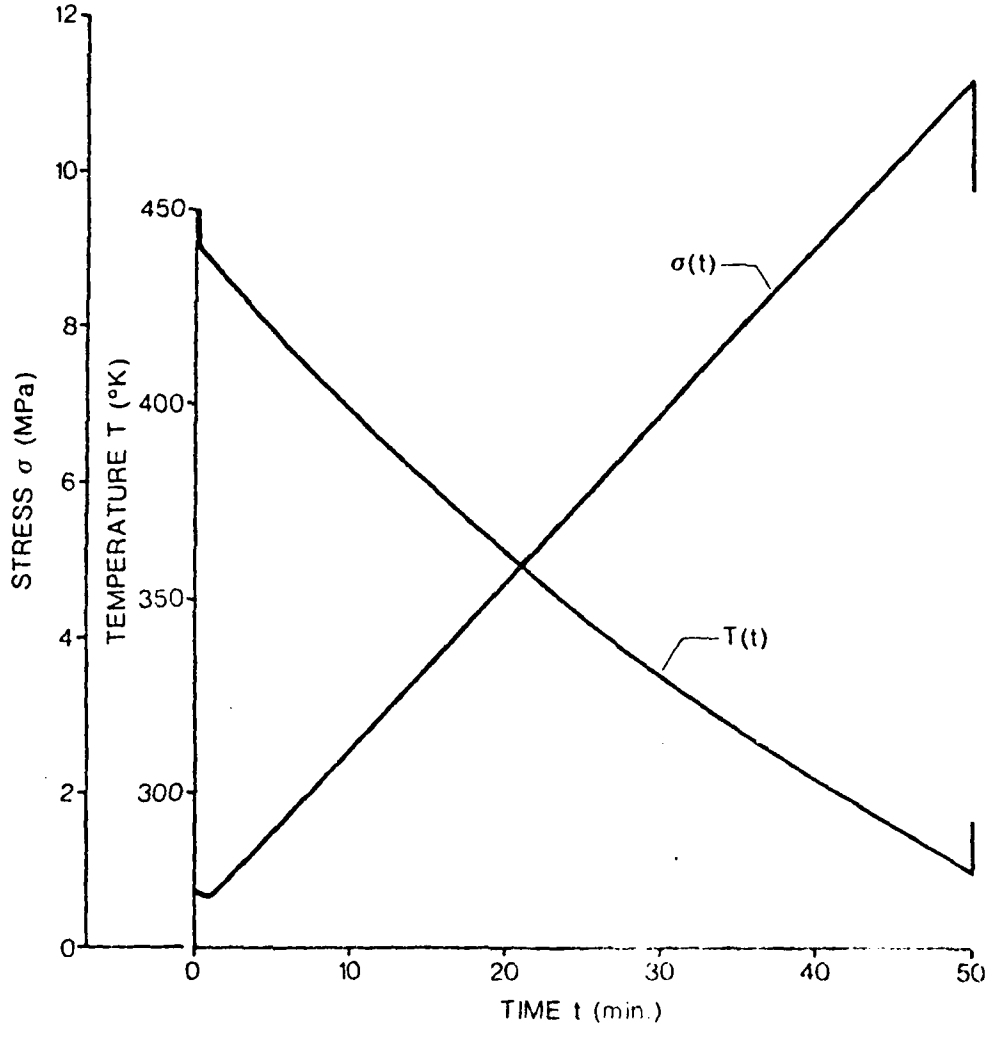

Fig. 1: The Optimal Cooling Path T(t) and the Accompanying Thermal Stress σ(t) vs. Time t for Epoxy/Aluminum Joints and Cooling Time t_f = 50 min.

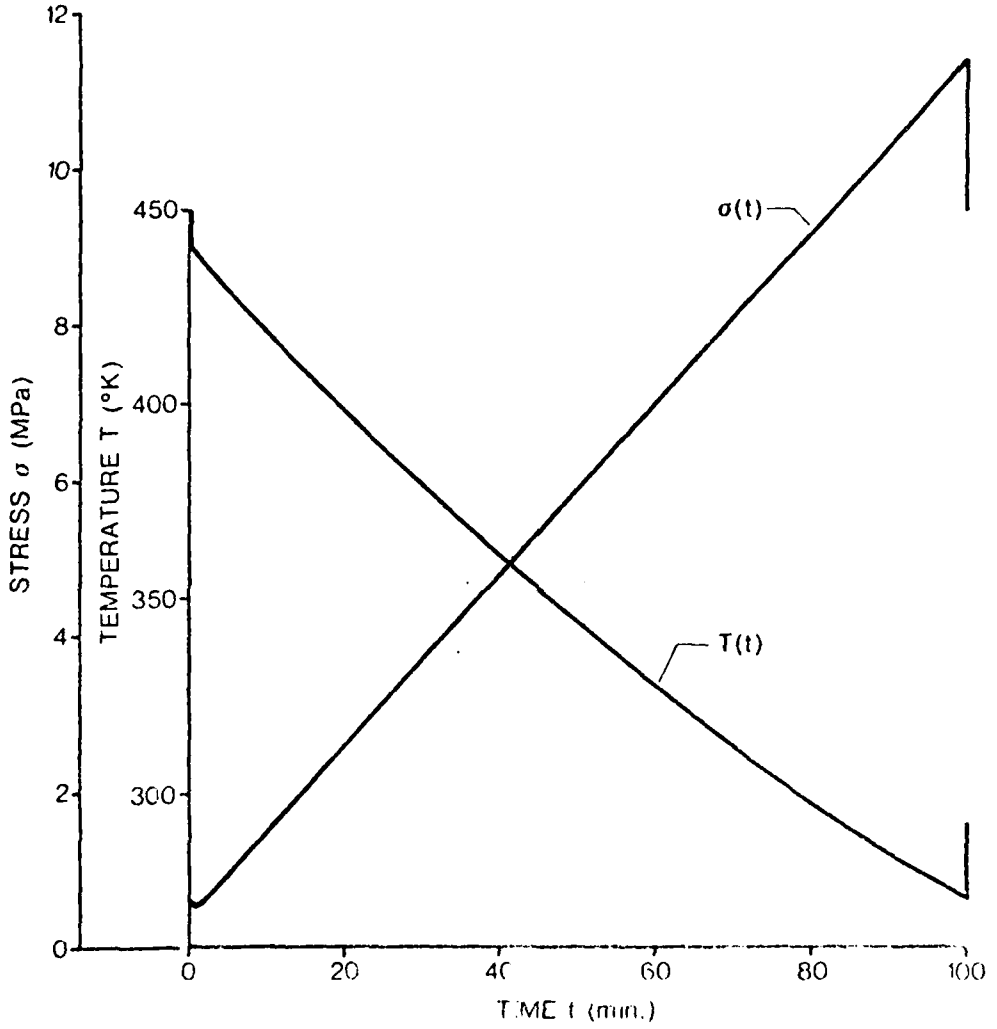

Fig. 2: The Optimal Cooling Path T(t) and the Accompanying Thermal Stress σ(t) vs. Time t for Epoxy/Aluminum Joints and Cooling Time t_f = 100 min.

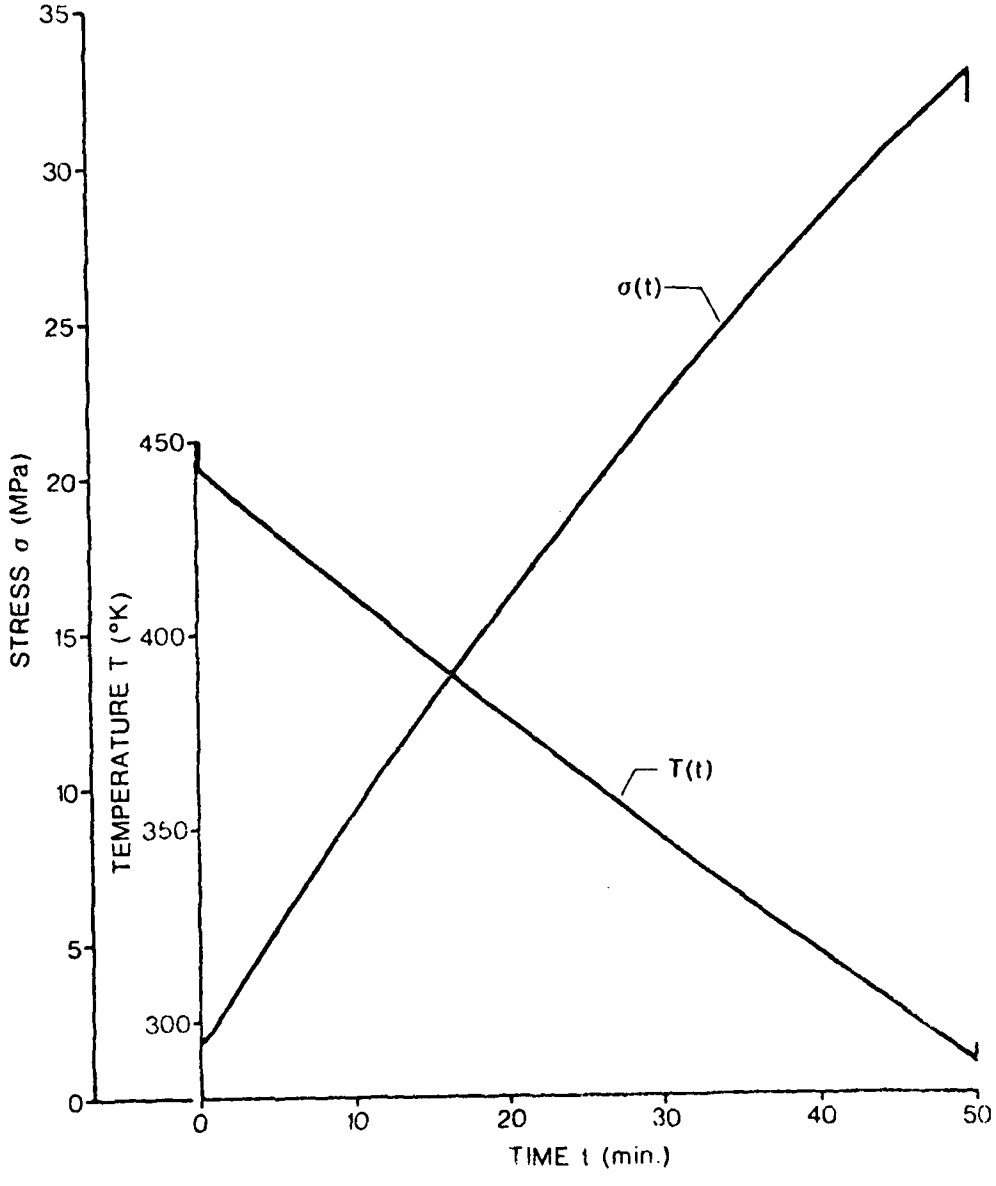

Fig. 3: The Optimal Cooling Path T(t) and the Accompanying Thermal Stress $\sigma(t)$ vs. Time t for T300/5208 Symmetric, Balanced 0°/90° Laminates and Cooling Time t_f = 50 min.

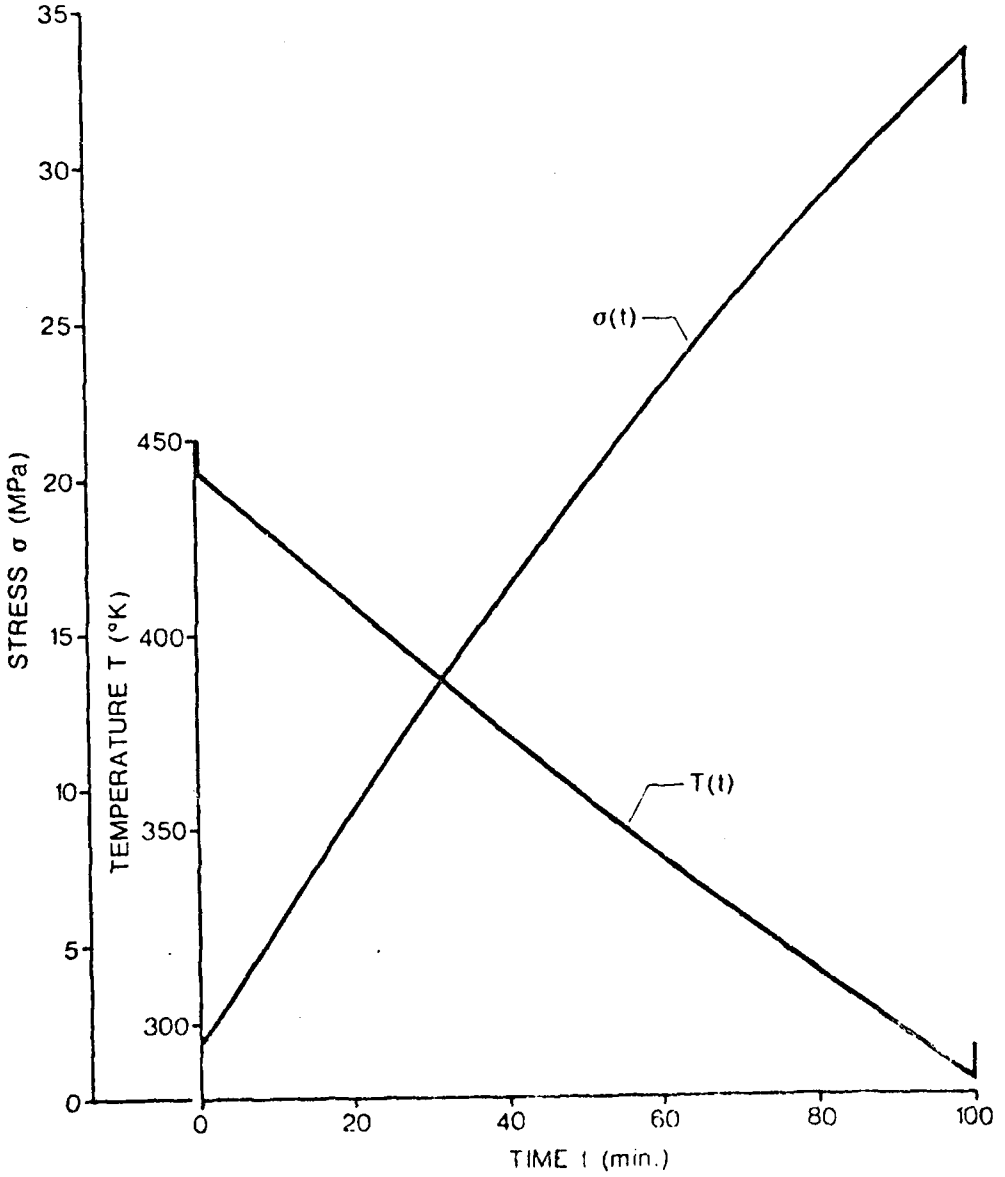

Fig. 4: The Optimal Cooling Path T(t) and the Accompanying Thermal Stress $\sigma(t)$ vs. Time t for T300/5208 Symmetric, Balanced 0°/90° Laminates and Cooling Time t_f = 100 min.

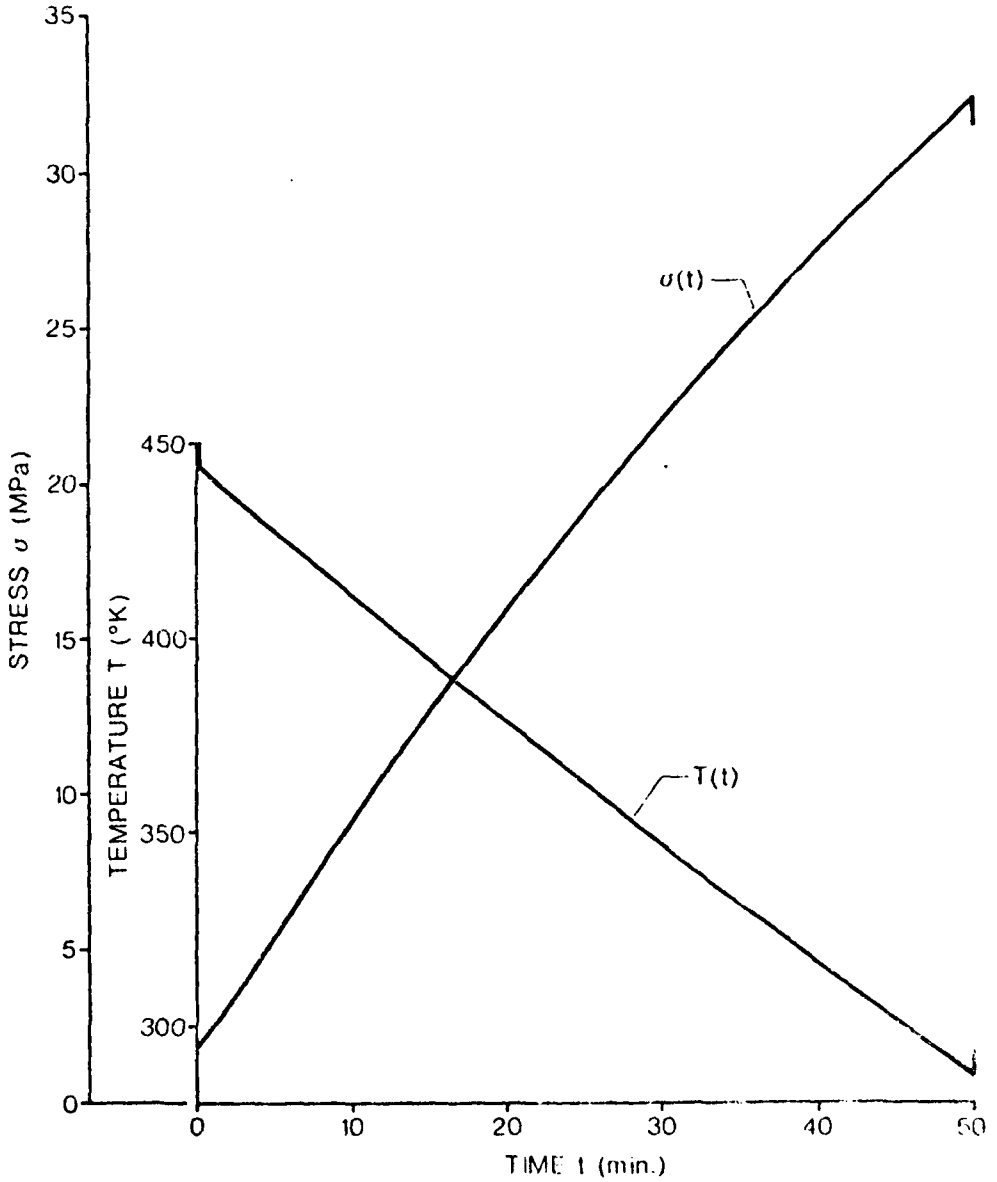

Fig. 5: The Optimal Cooling Path T(t) and the Accompanying Thermal Stress $\sigma(t)$ vs. Time t for AS/3502 Symmetric Balanced 0°/90° Laminates and Cooling Time t_f = 50 min.

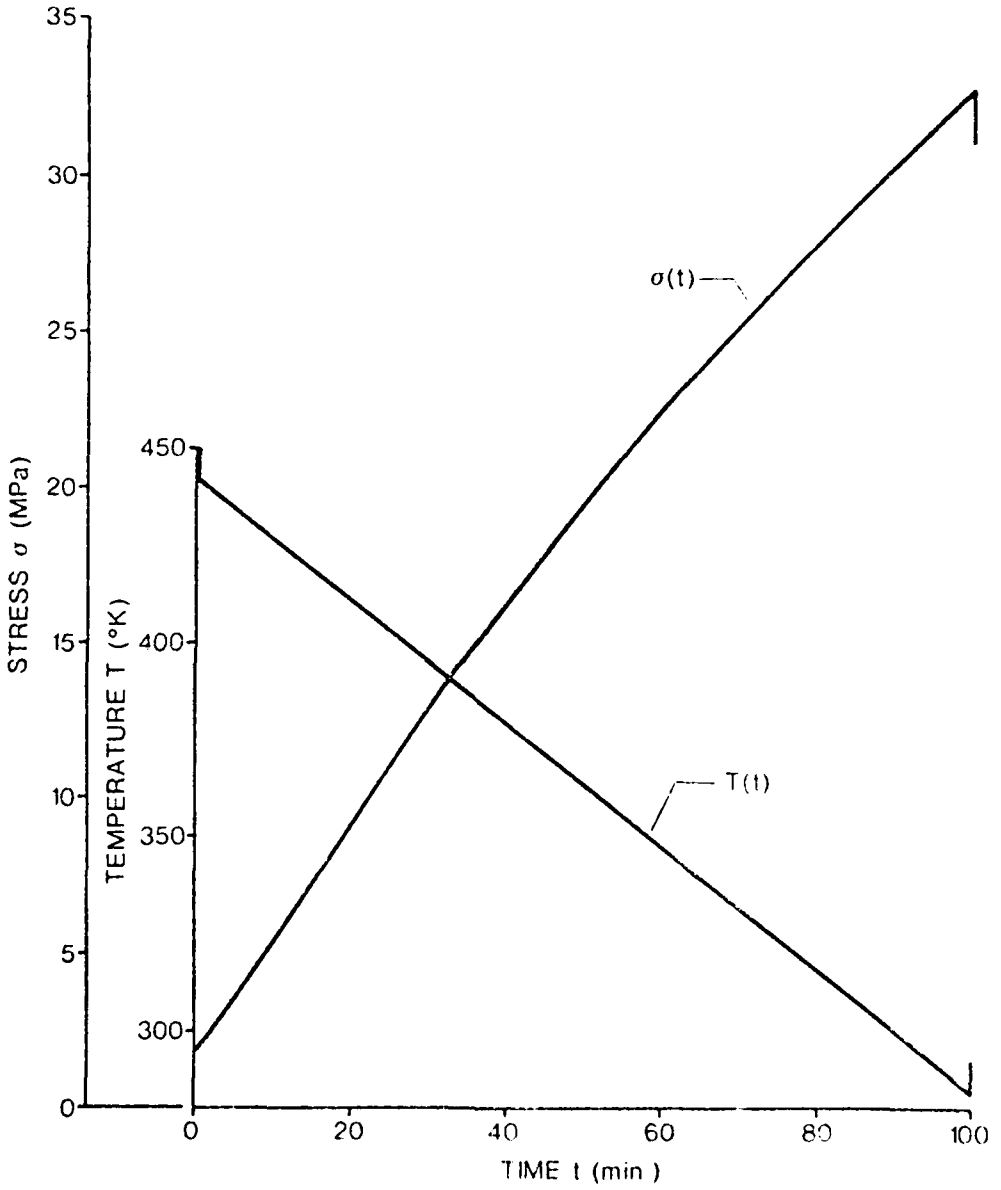

Fig. 6: The Optimal Cooling Path T(t) and the Accompanying Thermal Stress σ(t) vs. Time t for AS/3502 Symmetric, Balanced 0°/90° Laminates and Cooling Time t_f = 100 min.

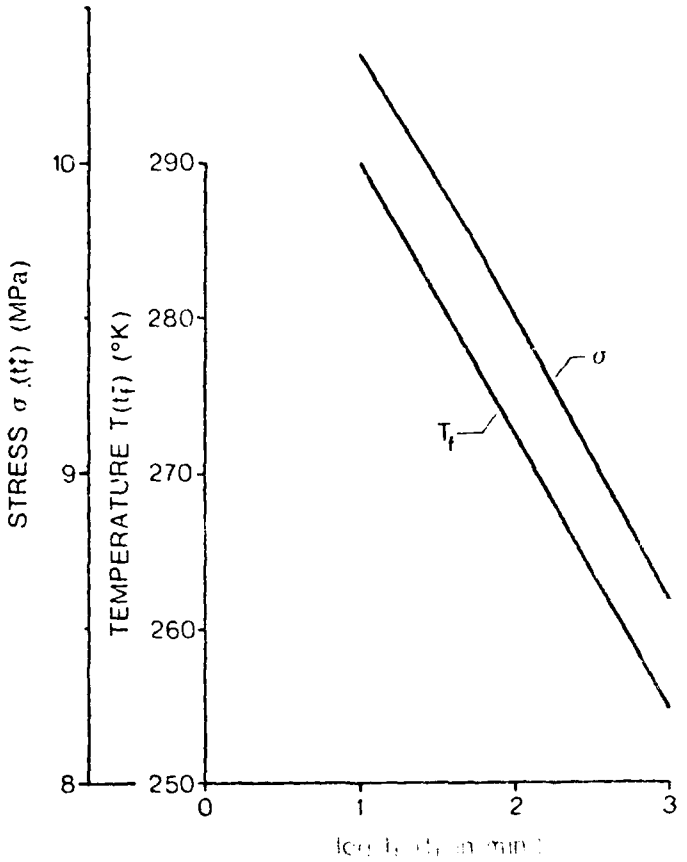

Fig. 7: The Variation of $T(t_f^-)$ and the Residual Thermal Stress $\sigma(t_f^+)$ vs. log t_f for Epoxy/Aluminum Joints.

AD-A122 262 COMPOSITE MATERIALS FOR STRUCTURAL DESIGN(U) TEXAS A AND M UNIV COLLEGE STATION MECHANICS AND MATERIALS RE.. W L BRADLEY ET AL. MAR 82 MM-3724-82-1 AFOSR-TR-82-1018

UNCLASSIFIED F49620-78-C-0034 F/G 11/4 NL

2/2

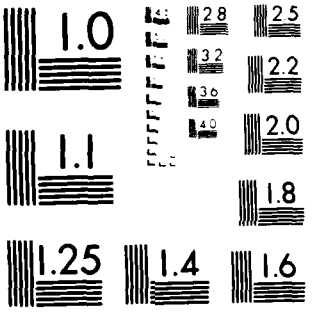

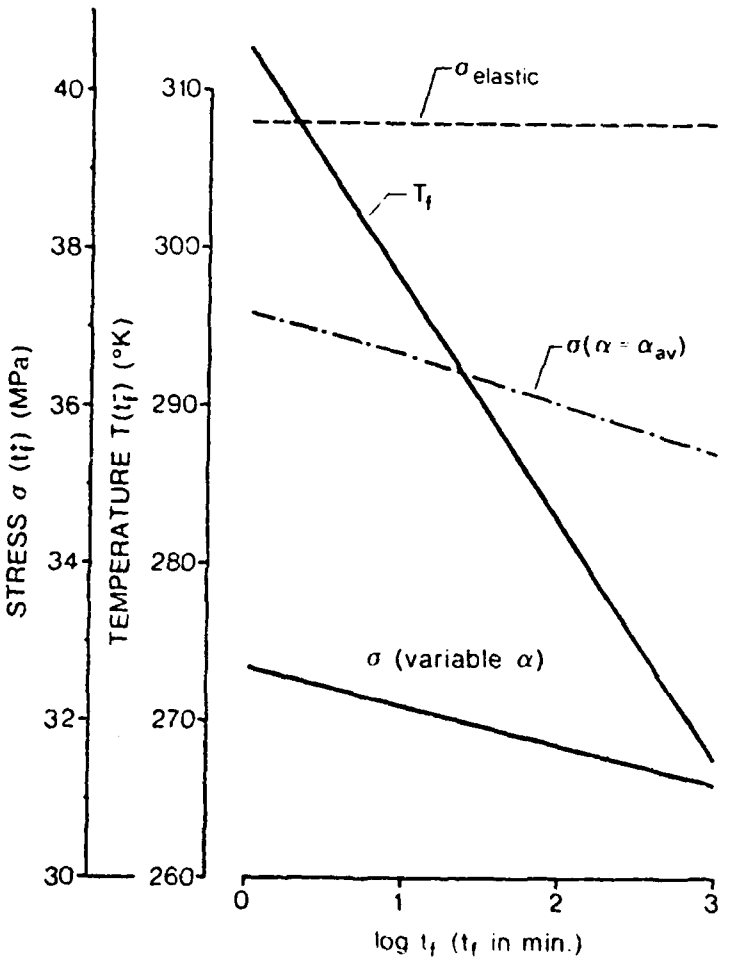

Fig. 8: The Variation of $T(t_f^-)$ and the Residual Thermal Stress $\sigma(t_f^+)$ vs. log t_f for the T300/5208 0°/90° Laminates. (The Dashed-Dotted Line Corresponds to $\sigma(t_f^+)$ evaluated with $\alpha = \alpha_{av}$.)

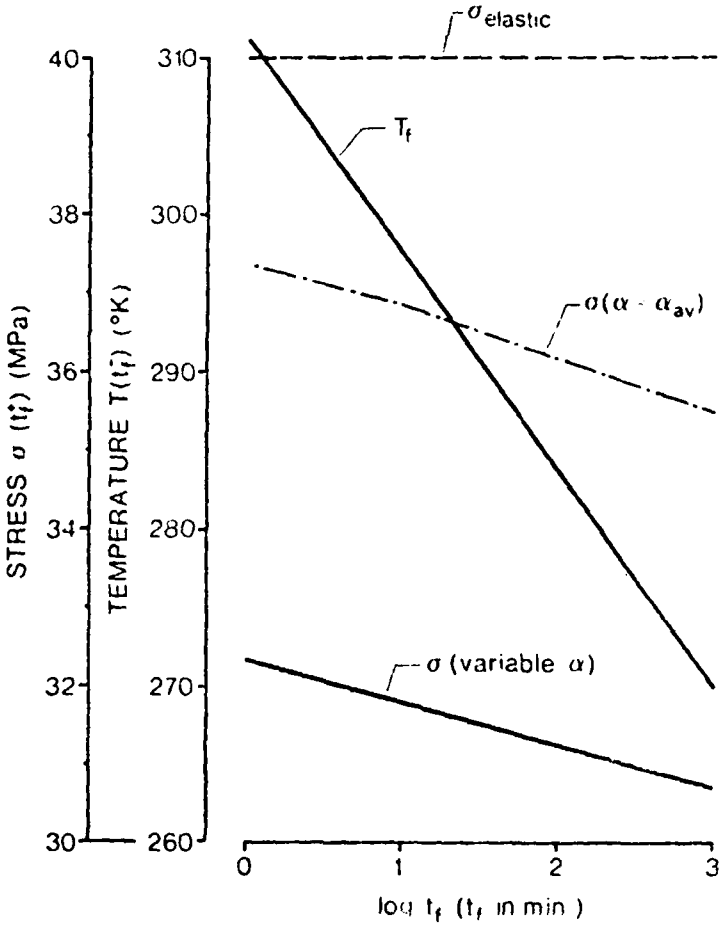

Fig. 9: The Variation of $T(t_f^-)$ and the Residual Thermal Stress $\sigma(t_f^+)$ vs. log t_f for the AS/3502 Laminates. (The Doshed-Dotted Line corresponds to $\sigma(t_f^+)$ evaluated with $\alpha = \alpha_{av}$.)

References

[1] Weitsman, Y., "Optimal Cool-Down in Linear Viscoelasticity", Journal of Applied Mechanics ASME, Vol. 47, No.1, pp. 35-39,(1980).

[2] Gurtin, M. E., Murphy, L. F., "Optimal Temperature Paths for Thermorheologically Simple Viscoelastic Materials", Quart. App. Math., Vol. 38, No. 2, pp. 179-190,(1980).

[3] Kibler, K. G., "Time-Dependent Environmental Behavior of Graphite/ Epoxy Composites". Technical Report AFWAL-TR-80-4052. General Dynamics Corporation, Fort Worth, Texas,(1980).

[4] Jones, R. M., "Mechanics of Composite Materials", Scripta Book Co., pp. 37-41, (1975).

[5] Tsai, S. W. and Hahn, H. T., "Introduction to Composite Materials", Technomic Publishing Co., pp. 8-18,(1980).

[6] Beckwith, S. W., "Viscoelastic Characterization of a Nonlinear Glass/Epoxy Composite Including the Effect of Damage", Ph.D. dissertation, Texas A&M University,(1974).

[7] Morland, L. W. and Lee, E. H., "Stress Analysis for Linear Viscoelastic Materials with Temperature Variation", Transactions of the Society of Rheology, Vol. 4, pp. 233-260, (1960).

APPENDIX B

Academic and Research Program Information


DAT
ILM